UNIVERSITY OF CALIFORNIA, SAN DIEGO

CHANGES IN ENSO TELECONNECTIONS UNDER GREENHOUSE-GAS FORCING: IMPLICATIONS FOR FISHERIES OFF THE WESTERN COAST OF SOUTH AMERICA

A thesis submitted in partial satisfaction of the

Requirement for the degree Master of Science

in

Oceanography

by

Gino Angelo Passalacqua Walter

Committee in charge:

Arthur J. Miller, Chair
Joel Norris
Bruce Cornuelle
David Pierce

2009

The thesis of Gino Angelo Passalacqua Walter is approved, and it is acceptable in quality and form for publication on microfilm and electronically:

Chair

University of California, San Diego

2009

DEDICATION

To Susan, for her endless love and support.

To my family in Peru, who with their love and support gave me the strength to keep fighting for my dreams.

To all the fishermen in Peru, who understand and deal with El Niño, the ocean and fish in a way that I could only imagine to achieve one day.

TABLE OF CONTENTS

Signature Page..... iii

Dedication…… iv

Table of Contents..... v

List of Figures……..... vii

Acknowledgments viii

Abstract ix

Chapter 1. Introduction ……..... 1

Chapter 2. Background

2.1 ENSO in Future Climate Scenarios …….. 6

2.2 Parallel Climate Model Main Characteristics …… 12

2.3 Brief Description of ENSO Effects on the Humboldt Current Ecosystem … 15

Chapter 3. Data and Methods …… 20

Chapter 4. Results and Discussion

4.1 Analysis and Results ……..26

4.2 Possible Effects on the HCE ……..... 32

4.3 Concluding Remarks ……..36

Figures ……39

Appendix

A. Ocean and Atmospheric Dynamics of the Southern East Pacific …… 52

B. Description of the Parallel Climate Model

B.1 The Parallel Climate Model ……...59

B.2 Atmospheric/Land Component ……61

B.3 Ocean Component …… 63

B.4 Sea Ice Component ……64

B.5 Model Initialization ……..65

B.6 PCM General Features ……..66

C. PCM Runs Description

C.1 Control Runs ……... 66

C.2 Historical Runs ……67

C.3 IPCC Runs …….. 68

References ……..70

LIST OF FIGURES

Figure 1. Map locating the indices created, with respective coordinates……. 39

Figure 2. First EOF of PCM SSTA for JFM seasonal averages of the CTRL ensemble, HIST ensemble, IPCC B2 and A2 scenarios……...40

Figure 3. Corresponding first PC (time series) of EOF patterns from Figure 2, for JFM seasonal average of PCM SSTA……41

Figure 4. First EOF of HadISST SSTA for JFM seasonal averages of the 1900-1949 and 1950-1999 periods…….. 42

Figure 5. Corresponding first PC (time series) of EOF patterns from Figure 4, for JFM seasonal average of HadISST SSTA…… 43

Figure 6. Frequency distribution of SSTA of PCM output of the JFM seasonal average of Nino 3.4 and South America 3 indices……44

Figure 7. Frequency distribution of SSTA of the HadISST data set of the JFM seasonal average of Nino 3.4, South America 2 and South America 3 indices……46

Figure 8. Schematic of the maps of difference in correlation of SSTA with the created indices…….. 47

Figure 9. Maps of difference in correlation of SSTA with the N34, SA2 and SA3 indices for the IPCC B2 scenario…… 48

Figure 10. Maps of difference in correlation of SSTA with the N34, SA2 and SA3 indices for the IPCC A2 scenario…… 50

ACKNOWLEDGMENTS

I give my greatest gratitude to my advisor Dr. Art Miller. His endless support, encouragement and enthusiasm made all the difference in my graduate studies. I am grateful for a valued friendship that he kindly extended to me. I am also thankful for his time and effort in reading my drafts. He conscientiously edited my terrible grammar and gave useful suggestions, which were essential to the completion of this thesis. Muchas Gracias, Art!

I would also like to thank my committee members: Joel Norris, David Pierce, John Roads and Bruce Cornuelle, for their service and contribution to my thesis research. Special thanks go to David Pierce, who always instigated my research with insightful, challenging questions and invaluable suggestions.

I also thank my fellow students, researchers, and friends at SIO, all of whom made my years here at SIO memorable and valued. Neil Gordon gave me an office to sit, his Matlab knowledge, and his priceless friendship.

I am extremely thankful with my parents and family in Peru for their continued support from distance. They have been my ultimate source of support and energy.

Finally, I would like to thank my wife, Susan. She has been always there, supporting and encouraging me, even when the end of this thesis seemed so far away. I am very thankful for her love, inspiring me to never give up and to follow my dreams.

ABSTRACT OF THE THESIS

Changes in ENSO Teleconnections Under Greenhouse-Gas Forcing: Implications For Fisheries Off The Western Coast Of South America

by

Gino Angelo Passalacqua Walter

Master of Science in Oceanography

University of California, San Diego, 2009

Arthur J. Miller, Chair

The Humboldt Current Ecosystem (HCE) is one of the most productive systems in the world. The interannual and interdecadal ocean-atmospheric variations in the Southeast Pacific (SEP) have recognized impacts on the HCE fisheries, especially during El Niño – Southern Oscillation (ENSO) events. To understand how anthropogenic climate change might affect HCE fisheries, the changes in teleconnections between the Peru/Chile coasts and the Pacific Ocean under these circumstances were investigated. Sea-surface temperature (SST) from the Parallel Climate Model (PCM) under the IPCC pre-industrial, 20th century and two future GHG scenarios were obtained to study these effects, by creating indices to identify the teleconnections.

We use EOFs to identify the warming trend spatial patterns, which are then removed to form detrended SST anomalies (SSTA) in order to examine ENSO statistics on a changing background state. We find an increase in the amplitude of the interannual

SSTA in the Nino 3.4 region and along the coast of the SEP in the PCM IPCC runs, corroborated with observations from the HADISST data set.

Atmospherically forced ENSO teleconnections broaden latitudinally and expand poleward under the influence of the trends in the background ocean-atmosphere state, independently from the IPCC scenario and the period of analysis. Under GHG forcing, there is a significant increase in correlations between the Equatorial Pacific and the SEP coast, especially in a region off Central / South Chile, indicating a poleward expansion of an “ENSO-like” pattern. Based on their historical responses to environmental variations, the possible effects of global warming on the HCE’s small pelagics fisheries are discussed.

CHAPTER 1

INTRODUCTION

The ocean-atmosphere coupled system plays an important role in the natural energy balance of the Earth. The atmospheric constituents tend to absorb the long wave radiation emitted by the Earth's surface and the ocean, and then reradiate it back to the surface producing what is referred to as the Greenhouse Effect (GHE), which is considered fundamental to maintain life on our planet. The two most important Greenhouse gases (GHG) in the atmosphere are water vapor and carbon dioxide ( ). The , after water vapor, is the GHG of greatest concentration in the atmosphere, contributing approximately 25% of the GHE and playing a principal role in determining the Earth's climate.

The fourth report of the Intergovernmental Panel on Climate Change (4AR) (IPCC, 2007) indicated that during the decades of 1940 and 1950, studies were carried out correlating the global warming with the increase of , attributed mostly to the burning of fossil fuels. The scientific community completely agrees that the noticeable increase of GHG concentrations (, methane and nitrous oxide) since 1750 is a direct result of human activities. The augmentation of concentrations in the ocean and atmosphere is due primarily to fossil fuel and land-use changes (IPCC, 2007).

The global atmospheric concentration has increased from the pre-industrial value of 280 ppm to approximately 375 ppm in 2005, exceeding considerably the natural range over the last 650,000 years (180 to 300 ppm) as determined from ice cores. The annual concentration growth rate has also increased since the beginning of continuous direct atmospheric measurements (in the late 50s), with a higher rate

averaged from 1995 to 2005, 1.9 ppm per year, if compared with the total record average from 1960 to 2005, 1.4 ppm per year (IPCC, 2007). The augmentation in GHG concentration produced a net radiative forcing of + 1.6 W m^{-2}, which translates into a total temperature increase from 1850-1899 to 2001-2005 of 0.76°C ± 0.19°C, where surface temperatures over land regions have warmed at a faster rate than over the oceans in both hemispheres (IPCC, 2007). In addition, the rate of warming averaged over the last 50 years (0.13°C ± 0.03°C per decade) is nearly twice that for the last 100 years, and the global surface temperature linear trend for the last 100 years has increased from 0.6 [0.4 to 0.8]°C (1901-2001) to 0.74 [0.56 to 0.92]°C (1906-2005) (IPCC, 2007, Solomon et al., 2007). Indisputable evidence has shown that the oceans have warmed since 1955, with a rate of warming in the shallower 0 to 700 m ocean layer of approximately about 0.5 ± 0.18 W m^{-2}, accounting for more than 80% of the changes in the energy content of the Earth's climate system (Solomon et al., 2007).

The Eastern Boundary Current (EBC) regions of the ocean, where coastal upwelling occurs, are extremely productive. Although their area makes up only 0.1 % of the world ocean, they account for 5 % of global primary production and 17 % of global fish catch (Pauly and Christensen, 1995). The EBC regions have very important fisheries (Bakun, 1996), among which small pelagics (mainly sardines and anchovies) are an important, if not major, component. Since anchovies and sardines are phytophagous at various points of their life cycle (Walsh et al., 1980; Pauly et al., 1989), the characteristic food chains are generally short with two or three components (Ryther, 1969; Margalef and Estrada, 1981; Pauly and Christensen, 1995). This implies both potentially high fish production and rapid response to environmental variability (Carr, 2002).

Among the EBCs, the area off the western coast of South America is the most productive due a combination of a wider shelf, upwelling all year, and proximity to the

equator (since Ekman transport is inversely related to latitude; Barber and Smith 1981; Bakun, 1996). In this region, the coastal waters of Peru (between 3 °S and 18 °S) are characterized by a large phytoplankton biomass and very productive fisheries (Carr and Broad, 2000).

An episodic warming off the Peru coastal waters has been recognized by the Peruvian fisherman for hundreds of years. They named this local SST warming “El Niño” in reference to the Christ child, due to its occurrence around Christmas time (Carranza 1891, Carillo 1892, Eguiguren 1894). Little did they understand that El Niño (EN) was a coupled ocean-atmosphere phenomenon occurring throughout the entire Pacific Ocean with considerable global consequences. The Peruvian coastal warming is generally the concluding feature of a series of ocean-atmosphere processes that begin in the western Pacific and propagate eastward. The EN events became noticeable to the scientific community in the 1890s (Philander 1990) but it was not until the mid-seventies that the warming along the Peruvian coast was linked to a large scale ocean-atmospheric event affecting the whole Pacific basin with global impacts (Bjerknes 1972, Wyrtki 1973, Wyrtki 1975, McPhaden et al. 2006).

It is now clear that ENSO is the major climate variation that impacts fisheries in the SEP region (Fielder, 2002; Niquen and Bouchon, 2007). The time has come to look at the future of fisheries through the identification and extrapolation of fundamental changes in ENSO under global warming scenarios. The goal of this thesis is to use a suite of GHG-forced global climate model simulations to identify how ENSO and its teleconnections may be altered in a GHG-warmed world.

Understanding the effects of GHG on ENSO and its effects on the SEP is a crucial task due to the significance of this area for ENSO generation and feedbacks, its importance to the large-scale Pacific ocean-atmospheric dynamics and the major impact

that ENSO has on the HCE fisheries, which is one of the most productive marine ecosystems in the world. Our hypothesis is that ENSO teleconnections under GHG forcing will be expanded poleward following a change of the background into an “ENSO-like” state (Zhang et al. 1997), due to alterations of the atmospheric circulation (Walker Cell and Hadley Cell, see Vecchi et al. 2006 and Vecchi & Soden 2007 for details on atmospheric circulation changes). We intend to show this expansion via a poleward increase of SSTA correlations between the SEP coast and the Equatorial Pacific, which generally has an “ENSO-like” correlation pattern. The main impacts on the SEP of those changes are more noticeable on the SSTA in central-southern Chile than in Peru. Based on historical records of EN effects on the HCE and our modeling results, we suggest consequences that these changes of the ENSO teleconnections could have on the HCE dynamics, which would translate into significant impacts on the fisheries in this region.

Gaining an understanding of the relationship between the ENSO, the environment, and fish, however, is no an easy task. Part of the problem is the lack of comprehensive data on marine environmental variables and fish distributions. The variable that has been used the most frequently to predict the distribution of fish catches is SST, because it is both a biologically important variable and one that is available with good spatial and temporal resolution from three decades of satellite generated data. There are many examples in the literature where catches and the distribution of large and small pelagic fish (tuna, swordfish, anchovy, sardines, herring, etc) have been related to SST and SST fronts (Williams 1977, Stretta 1977, Laurs et al. 1984, Fiedler & Bernard 1987, Maravelias & Reid, 1995, Castillo et al. 1996, Van der Lingen et al. 2001, Agenbag et al. 2003), which are clearly influenced by climate events like ENSO.

Understanding the possible effects of changes in ENSO due to global warming on commercially significant fish populations is an important task. By providing this

information to the institutions that manage their fisheries, ENSO and global warming effects could be included in the yearly fisheries management strategies, in order to plan environmentally and economically sustainable exploitation of the resources. This will facilitate the mitigation of the negative impacts on individuals whose live depends on fishing and take advantage of the potentially positive impacts of global warming.

CHAPTER 2

BACKGROUND

2.1. ENSO in Future Climate Scenarios

The ENSO event is the dominant mode of coupled atmospheric-ocean variability on interannual timescales in the Pacific Ocean, with important consequences over the whole planet. Understanding and predicting ENSO occurrence and amplitude, on seasonal time scales and for the next century, has become an important matter for societal needs.

The chronological evolution, amplitude, the relative importance of the mechanism, feedbacks, spatial patterns of ENSO vary for each event. The interaction of ENSO with the basic state and seasonal cycle are significant factors for its progression. These are elements that must be taken into account for ENSO predictions both on an interannual timeframe and for predictions under a future global warming scenario. There has been a vast variety of studies describing the changes of the mean state of the tropical Pacific and the variation of ENSO dynamics and statistics under GHG forcing, with an interesting mixture of conclusions. Here we present a short review of these studies.

The east-west asymmetry over the Pacific Ocean of sea surface temperature (SST), thermocline depth, time-averaged cloudiness, rainfall and atmospheric circulation are attributable to easterly winds that depend on global circulation patterns (see appendix A for a detailed discussion of the SEP climate). Changes of these and other processes that constitute the EN background state has generated a debate on the

possibly significant effects of GHG forcing on ENSO. As evidence of possible effects, a change has been noticed in the SSTA spread during ENSO events from a westward propagation in the 1960s and 1970s to a more common eastward propagation starting on ENSO 1982 (Fedorov & Philander, 2000).

Timmerman et al. (1999), using a model simulation with the IPCC scenario IS92a, suggested a change in the mean climate in the tropical Pacific region towards a state similar to present-day EN conditions, due to a strengthening of the equatorial thermocline, leading to a more frequent occurrence of EN events. Also, he suggested a stronger interannual variability leading to more extreme year-to-year variations with stronger cold events relative to the mean "warmer" state.

Timmerman (2001), with the same model setup, noticed no significant trend in ENSO frequency under greenhouse forcing, a tendency of EN events to occur more to the east and a change from a stable oscillatory regime to an unstable one, similar to the change that occurred in between the 70s and 80s. Those changes were accompanied by a decadal shift in the amplitude, structure and frequency of ENSO (An & Jin, 2000, An & Wang, 2000). The changes in ENSO stability are attributed to modifications in the ocean dynamics, interpreted as variations in the relation between Kelvin waves, off-equatorial Rossby wave initiation and ENSO related sea surface temperature anomalies (SSTA) patterns.

Cane (2005), based on paleoclimate records (corals, tree ring reconstructions and lakes' laminated cores) and model studies, concluded that ENSO behavior is quite sensitive to climatological conditions. He inferred that if the east-west temperature gradient is weaker (possible scenario under GHG forcing), the winds will slacken, causing a further decrease in the temperature gradient – the Bjerknes feedback - leading to a more El Niño-like state. This state has been confirmed by Vecchi et al. (2006), who

discovered a weakening in the Walker circulation, based on historical observations of SLP and GCMs. In their study, the trend indicates a reduced zonal SLP gradient, and consequently a weakening of the zonal atmospheric circulation. In addition, Boer et al. (2004), examining coupled models, feedback analysis in the tropical Pacific, and observation-based paleoclimate reconstructions, suggest a mean “El Niño-like” temperature response to positive radiative forcing due to an increase in atmospheric greenhouse gases. This statement contradicts Clement’s results of a “La Niña-like” conditions, but this is basically due to the difference in the mechanism proposed for Clement's “La Nina-like” response (Vecchi et al., 2008).

When looking into ENSO’s characteristics (periodicity and base amplitude) and regularity in coupled GCMs, the atmospheric component plays a governing role. The resolution of the atmospheric model and even the coupling strengths between the atmospheric and ocean component of the GCM, primarily creates significant differences between coupled models that share the same ocean component, whose role in setting the frequency characteristics of ENSO appears to be less important (Philip and Van Oldenborgh, 2006). However, for the ENSO amplitude the ocean component has a greater role (Guilyardi et al., 2004). This conclusion was supported by Meehl et al. (2004) who analyzed the factors affecting climate sensitivity in GCMs by comparing four models. They highlight the “managing” role of the atmospheric component relevant to global feedbacks, including sea ice albedo, water vapor, clouds and ocean heat uptake (due to changes in surface fluxes of heat and freshwater, affecting the ocean’s surface density). But the ocean, sea ice and land surface components could have more relevant roles than the atmospheric component in regional climate changes.

With the idea of comparing EN in global coupled climate models by isolating possible contributions from various factors, Meehl et al. (2001) analyze different versions

of the coupled Climate System Model (CSM) and the Parallel Climate Model (PCM). They determine that the amplitude of EN variability is greater with a lower value of ocean background vertical diffusivity. The amplitude is largely related to a sharper equatorial thermocline (Meehl et al., 2001). Among the models with low background vertical diffusivity, stronger equatorial zonal wind stress produces a more realistic east-west SST gradient and a higher amplitude EN variability. The known error in GCMs of a double permanent ITCZ and too much of a semiannual SST seasonal cycle in the eastern tropical Pacific did not affect the amplitude of the EN variability.

In many regions of the world, climate projections for the next century are strongly associated with potential changes in the properties of ENSO, therefore a significant effort in the modeling community has being directed towards multi-model studies to determine if an “El Niño-like” or “La Niña-like” state will occur in future climate under GHG forcing (for definitions of “El Niño-like” or “La Niña-like”, see Collins et al. 2005). Using a probabilistic prediction of “ENSOness”, Collins et al. (2005) concluded that the most probable scenario is no strong trend toward either EN or LN conditions. The second more probable was a slight trend towards an “El Niño-like” scenario. In this study, an “ENSO simulation Index” was used to equally weight the ability of the models to simulate either mean climate or ENSO variability, observing that the models with larger “El Niño-like” climate change have the poorest simulation in ENSO variability.

In a study for the IPCC AR4, by comparing 19 models with observations, van Oldenborgh et al. (2005), based on a pressure index, found no statistically significant change in the amplitude of ENSO variability in the future, with changes in the standard deviation of the SOI that are no larger than observed decadal variations. Based on the large uncertainties and skewness of the variability, this multi-model ensemble analysis expects a very modest influence of global warming on ENSO. Specifically, for the PCM

future scenarios, van Oldenborgh et al. (2005) found a more “La Niña-like” mean condition, but it was assigned a lower confidence due to its low-resolution and an overly surface-driven cycle. It is proposed that this change is due to a large increase in SSTs in the Indian Ocean or off-equatorial Pacific Ocean projecting onto the ENSO pattern. It is important to mention that this study did not incorporate coastal EN (our area of interest) due to poor resemblance of the models to observations, presumably because the thermocline is too deep as a consequence of the lack of realistic stratus clouds, and also because the narrow coastal upwelling signal cannot be captured by GCMs due to their poor resolution.

Meehl et al. (2006) published a meticulous study of the changes of ENSO under IPCC AR4 scenarios for two models, the PCM and the Community Climate System Model Version 3 (CCSM3).A description of their results is presented in this section, due to the importance of their results (based on the PCM) for our research. Their study was focused on the assessment of ENSO properties in Control scenarios versus 2 x , 4 x and transient scenarios.

Washington et al. (2000) established with the PCM model that EN and LN events in the tropical Pacific have the variability and amplitude similar to the observed. The power spectrum of Niño3.4 SST for the PCM is concentrated towards higher ENSO frequencies from 2 to 4 years, in comparison to observations that have 2.5 – 7 years period (Meehl et al., 2001). Under higher positive radiative forcing the PCM shows a decrease in power on the Nino3.4 frequency distribution with a bigger decrease as the forcing is increased. In addition, the Niño3.4 variability decreases with increasing positive radiative forcing. The amplitude of ENSO for 2 x and 4 x is reduced when compared with control runs. However, the amplitude change for transient scenarios in PCM is negligible. Only under the 4 x forcing are the changes in the amplitude

significant at the 10% level (Meehl et al., 2006). These variations are likely related to different slopes of the thermocline among runs, which would affect the amplitude of ENSO (Meehl et al., 2001).

Changes in ENSO teleconnections have so far not been detected in observations since the late 1800s, but have been noticed in some climate models under GHG forced scenarios over long periods of time (more than a century) suggesting that the signal is weak compared to natural variability (Sterl et al., 2007).

When analyzing ENSO teleconnections in PCM, Meehl et al. (2006) compared the effects of strong events versus moderate events by analyzing SLP anomalies during the months of December, January and February, concluding that a reduction of ENSO amplitude contributes to weaker midlatitude teleconnections for North and South America.

Meehl and Teng (2007) showed with a multi-model ensemble that ENSO's SLP teleconnections were stronger in the Southern Hemisphere, when compared with the Northern Hemisphere. The former teleconnections are characterized by negative SLP anomalies in the region of 40° S to 60° S, and positive anomalies south of 60° S in both the observations and models. Having said this, they emphasize that changes of future ENSO teleconnections with regard to SLP anomalies will depend on whether models project a future increase or decrease of ENSO amplitude and the magnitude of the GHG forcing. In the case of temperature variations associated with these changes in SLP teleconnections, the greater the GHG forcing, the larger the changes will be in temperature. It is worth remarking that changes in the basic state circulation will also play a very significant role in the changes in future ENSO teleconnections. In the case of ENSO teleconnections over North America, the changes in the basic state circulation

with increasing CO2 has the most consistent influence and also is the least model dependent.

An important aspect of ENSO that has been neglected in these published studies is the detailed structure of the ENSO teleconnections that may occur in future climate conditions and their potential impact on fisheries. Do the teleconnection patterns change markedly, thereby affecting areas that are currently only weakly influenced by ENSO? What physical oceanographic features are associated with these possible teleconnection changes and how might they consequently influence fisheries in future climate conditions? We will explore these issues by using the PCM suite of climate simulations.

2.2. Parallel Climate Model Characteristics

The PCM is a global coupled ocean-atmosphere-ice model that has been used in numerous GHG-forced global warming scenarios and is one of the IPCC AR4 models (see Appendix B for model details). Here we discuss the characteristics of the ocean-atmosphere dynamics of the PCM, obtained from reviewing various scientific publications, as well as the response of certain variables (mean air temperature, sea level rise, etc.) under different experiments. It is essential to mention that most of the investigations done for the PCM were completed with multi-model studies; that most of these studies focus generally on surface properties of the ocean on global scales or in the Equatorial Pacific region; and finally, none of these studies extensively investigate the Southern Pacific Ocean or the western coast of South America.

In general, the PCM represents properly the surface temperature and sea level patterns and their seasonal cycle, when compared to observations. Although, the model is generally colder than observed, especially in the winter hemisphere and the Southern

Hemisphere, surface temperatures are too warm by several degrees areas along the coast of western South America (Washington et al., 2000).

The warming patterns represented by future scenarios of the PCM are very similar to previous climate change experiments from other GCMs, with greater warming at high latitudes in the winter hemisphere than in the summer hemisphere, mostly due to problems with the sea-ice component of the model. It is important to mention that the PCM is one of the least sensitive of the AR4 models (see Table 8.2, from the IPCC AR4 report: IPCC, 2007)

The atmospheric component of PCM, the CCM3, experiences a systematic error in zonal wind stress, which is too strong in the eastern equatorial Pacific. This error is perceptible in the coupled simulation in the central and western Pacific. The bias created by the wind stress with stronger easterlies, normally present in global couple models, translates into a further westward extension of the cold tongue regime, extending across the entire Pacific penetrating well into the western Pacific warm pool. Consequently, in contrast with observations, it results in a westward shift of the ascending branch of the Walker circulation in the western Pacific and related errors in the eastern equatorial Indian Ocean (Meehl et al., 2001).

In addition, the PCM has a stronger ITCZ north of the equator during the second half of the year, and a double ITCZ during the northern spring. More significantly, the model tends to fabricate a southern ITCZ year round, predominantly stronger in northern spring, with a maximum located farther poleward, 10-12° S in northern spring, and around 10-12° N for the northern ITCZ compared to about 5° S and 8-10° N, respectively, for the observations. However, this is a distinctive problem in many global coupled models without flux adjustment. Yu and Mechoso (1999) partly attribute this problem to the inaccurate simulation of the stratus clouds off the coast of South America,

or with specifics of the convective parametrization and the resulting SST errors south of the equator in the eastern Pacific.

As a general characteristic, the PCM has in the Central Pacific a shallower Equatorial thermocline depth of 50 m, compared to a thermocline depth of 120 m in the observations, reflecting a colder SST at the surface, and systematic error of colder than observed temperatures in the upper 400 m, which is manifested by a 20°C isotherm being near the top of the thermocline. Both the depth of the thermocline and its intensity, are important factors in determining the Nino3 region SST amplitude (Nino3 SST amplitude is a common index to measure the intensity of ENSO). Nevertheless, models with a systematic upper ocean bias tend to do a reasonable job simulating observed Nino3 amplitudes. However, Nino3 amplitude by itself does not fundamentally represent all ENSO-related characteristics of climate models (Meehl et al., 2001).

In a multi-model study of the effects of global warming on ENSO, van Oldenborgh et al. (2005) determined that PCM has a too short ENSO period. By calculating the first normalized Empirical Orthogonal function (EOF) of observed SST anomalies, they found an amplitude of 0.25 and skewness of 0.54, meaning that SST anomalies are in general larger than during EN than during LN. In contrast the PCM has an amplitude of 0.23 and skewness of 0.21. In addition, the PCM showed hardly any response to easterly wind anomalies in the west, central and eastern Pacific. This weak response explains why the thermocline variability is lower that observed; it also produces a suppression of the non-linear aspects of ENSO in the ocean (for details see reference). Also, the PCM has too strong wind sensitivities in the Central Pacific to compensate for the weak wind response. As the thermocline feedback is not enhanced, this implies that ENSO in the model is much more surface-driven than in observations.

The ENSO events in the PCM are described mostly by SST-mode event type, however some thermocline mode events occur in the model (Meehl et al., 2001). ENSO events have lower amplitude, the warmer and more diffuse the thermocline is (Meehl et al., 2001). Arblaster et al. (2002) showed that a deeper, warmer thermocline in the PCM produced lower amplitude ENSO events during warm periods in the tropical Pacific on the multi-decadal timescale, while a cooler, more shallow thermocline produced higher amplitude ENSO events on that timescale.

2.3. Brief Description of ENSO Effects on the Humboldt Current Ecosystem

Fish behavior, biomass and distribution in the EBCs are influenced by seasonal, interannual and decadal climate variations (Lluch-Belda et al. 1989, Bakun and Broad 2003, Chavez et al. 2003, Alheit & Niquen 2004, Bertrand et al. 2004). Along the SEP, interannual variability due to ENSO is contemplated to be one of the major sources of variability (Schwartzlose et al. 1999; Yañez et al. 2001; Fiedler 2002; Stenseth et al. 2002; Chavez et al. 2003). ENSO events affect all the components of the marine ecosystems (e.g. Barber and Chavez 1983, Ulloa et al. 2001, Fiedler 2002, for a review, Escribano et al. 2004). The HCE has the highest fish landings of all EBCs, but it appears that higher fish catches are not directly related to higher primary productivity (Carr, 2002; Carr and Kearns, 2003). One of the main factors that could influence higher fish catches is the exposure of the HCE to high climatic stress at several spatio-temporal scales, directly influenced by the ENSO cycle between EN and LN years (Alheit & Niquen 2004, Bertrand et al. 2004). Apparently, EN events “reset” the HCE dynamics, making only the stronger individuals to survive in marine environments. In addition, marine species in the HCE have developed spatial and temporal adaptive strategies to mitigate strong

unfavorable conditions, especially small pelagics (Arntz and Fahrbach 1996). Therefore, EN events could be the secret underlying the extreme fish productivity of the HCE, instead of the general perception of negatively affecting fish populations (Bakun and Broad 2003). In the HCE, 'variability is normality' (M. Espino, personal communication).

Even though ENSO effects on fish populations produces various types of responses (Niquen and Bouchon, 2004), the common belief is that EN produces considerable die-offs of anchovy. However, the biomass of sardines, jack mackerel (*Trachurus murphyi*, Carangidae) and mackerel (*Scomber japonicus*, Scombridae) generally increase during and after EN events (Pauly and Tsukayama 1987; Arntz and Fahrbach 1996). In the last few EN events, anchovy biomass was reduced significantly, but, the recovery pattern afterwards was not always the same (Bakun and Broad 2003; Alheit and Niquen 2004, Niquen and Bouchon, 2004). Anchovy biomass slowly recovered after EN events in 1972–73, 1977–78 and 1982–83, but it had a speedy recovery after the EN of 1987 and 1997–98. On the other hand, anchovy biomass did not have a perceptible decrease during the EN of 1992–93 and 2002–03 (Gutierrez et al. 2007). It's important to mention that different fishing regulations between the years may partially explain such differences, as more precautionary management approaches have been implemented since the mid-1980s (Csirke et al.1996), specially after the 1997-98 event. Generally, anchovies tend to migrate south and go deeper, out of range from the fishing nets, but during ENSO 1997-98 a strict control was implemented on the fisheries (based on the oceanographic conditions) to avoid overfishing and or juveniles catches (Alheit and Niquen 2004, Niquen and Bouchon 2004, Bertrand et al. 2004, Gutierrez et al. 2007).

Oceanographic changes associated with EN include Kelvin waves towards and along the coast and a rise of the near-shore sea level in the eastern Pacific connected

with a deepening of the thermocline. Thus upwelling takes place only in the mixed layer without returning nutrients from the bottom water to the surface layer (Barber and Chavez 1983). Other important effects for the marine biota include an increment of the SST (in extreme EN years up to 10°C) during several weeks, alterations in water circulation and hence changes in advection, an increase of dissolved oxygen concentration at the normally hypoxic soft bottoms of the Oxygen Minimum Zone (OMZ), agitated sea and changes in UV radiation (Tarazona & Arntz 2001, Alheit & Niquen 2004, Niquen & Bouchon 2004). Arid regions of Peru and Chile receive tremendously increased rainfall during strong ENs, causing flash floods, river inundations, erosion, mudflows, and landslides. The flood-transported sediments, waterworks, roads, and cropland (Glantz 1984, Orlove et al. 2004). The significant increase of fresh water input (which changes the surface salinity), the increased sediment load and associated nutrients to the coastal system is a major boundary condition for the near-shore marine ecosystem. These oceanographic changes have drastic effects on the marine biota. However, the changes to the ecosystem depends on the time of onset of the EN event, its duration and intensity along the equator and its anomalies projections towards coastal areas, the distance from the events main impact zone, the species composition during the period before the development of the phenomenon and other factors. The 1982–1983 EN event started in austral spring, just before the reproductive season and showed much stronger effects biological effects on the HCE, than the EN 1997–1998 starting in austral autumn (Niquen et al. 2000, Bertrand et al. 2004, Niquen & Bouchon 2004, Arntz et al. 2006).

An additional crucial issue to interpretation is to place ENSO in the context of observed decadal oscillations with a period of about 50 years, even if the exact timing of shifts is still controversial (Lluch-Belda et al. 1992; Clarke and Lebedev 1999; Yañez et

al. 2001; Fiedler 2002; McFarlane et al. 2002; Chavez et al. 2003; Alheit and Niquen 2004, Bertrand et al. 2004). The terms ‘El Viejo’ and La Vieja’ were used to define a warm, ‘sardine regimes’ between 1925 and 1950 and from 1975 to the mid-1990s, and a cold ‘anchovy regimes’ from 1900 to 1925, 1950 to 1975, and probably after the mid-1990s, respectively (Chavez et al. 2003). Along the Peruvian coast, zooplankton volumes were higher during cold decades than during warm decades. After the EN 1972-73, zooplankton volumes never recovered to the levels previous to the event (Ayon et al. 2004). Nevertheless, anchovy biomass recovered in 1995-96 to similar levels previous to the now famous collapse of the Peruvian fisheries as a consequence of EN 1972-73.

The 1997-98 EN happened during a long-term cold ‘anchovy regime’, even if its magnitude and extent was comparable with the EN of 1982-83. During this warm event, anchovies found finding small scale ‘loopholes’, (Bakun and Broad 2003), maybe allowing them to recover their biomass rapidly after the event. However, anchovy biomass decreased robustly from the end of 1997 (5.8 million tons) to a minimum of 1.2 million tons during the survey of August to September 1998. At the beginning of 1999 anchovy biomass increased to 5.2 million tons. These variations in biomass were characterized by changes in horizontal distribution, without robust latitudinal migration (as in previous events), and was distributed almost all along the coast of Peru and northern Chile, with higher concentration south of 8° S. Anchovies were distributed very close to the shore until the end of 1998, migrating offshore afterwards (Bertrand et al. 2004). During the EN period, distribution of sardine, jack mackerel and mackerel (all species displaying a distribution area larger than the Peruvian Exclusive Economic Zone (EEZ) followed the oceanic water flux towards the coast. After the El Niño–La Niña shift,

these fish rapidly dispersed and almost disappeared off the Peruvian coast (Gutierrez et al. 2007).

CHAPTER 3

DATA AND METHODS

Our objective is to use the PCM output to quantify the structure of ENSO ocean-atmosphere teleconnections in control climate (pre-industrial), historical climate (century) and future climate (century) scenarios. Here we describe the techniques we use to analyze the PCM outputs with the intention of removing trends, defining teleconnection indices and patterns, and distinguishing the effects of the different climate scenarios.

The data was obtained from the DOE PCM model, thru the Earth System Grid web page downloading system (https://www.earthsystemgrid.org/); a period of 50 years was used for the analysis of each different run. The model output has monthly averages for each variable. Seasonal averages were made for the months of January, February and March (JFM), when the ENSO SST anomalies are the strongest (Joseph and Nigam, 2005). In addition, the months of July, August and September (JAS) were considered as seasonal average, to investigate the changes in the ocean-atmosphere dynamics during the Austral winter. It's important to mention that these two seasons are banned from anchovy fishing in most of the west coast of South America to protect the spawning and recruitment of the specie.

The atmospheric and ocean outputs of the model were analyzed during this research. Here, only the ocean output analysis is presented. Maps of monthly ocean temperature anomalies (OTA) were calculated for each run by subtracting 50 years climatology from the ocean temperature at different depths. The OTA were smoothed

with a double 5-month running-mean filter to emphasize interannual variability (Shu & Clarke, 2001; Zhang & McPhaden, 2006).

We used five 50 years periods of two different PCM Control runs, B06.18 and B06.62 (see Appendix B for details on each run); each one of them spaced by at least 20 years, to create an OTA Control Ensemble average (CTRL). We also create an OTA Historical Ensemble average (HIST) from three different PCM historical GHS, sulfate and ozone forced runs (B06.08, B06.22, B06.23). The period for the HIST was from 1950 to 1999 (for details of each PCM model run, see Appendix C). The different runs utilized in the HIST were created by branching off a long control run at different points and by running those branches with anthropogenic forcing. Averaging over all ensemble members reduces the random, internally generated climate variations, producing an estimate of the externally forced climate signal (Selten et al. 2004).

For the future runs, two IPCC scenarios were chosen. These selected runs represent the boundaries of the spectrum of possible future states of the emissions, Earth's development, global temperature and sea level increases. The PCM future runs chosen are the IPCC B2 (PCM B06.21), scenario that forecast a mild/moderate increase of the global temperature, and the IPCC A2 scenario (PCM B06.20), which is one of the more aggressive forecasts for future global temperature increases. For each IPCC run, a period of one hundred was analyzed, subdividing each run in two consecutive periods of 50 years, from the years 2000 to 2049, from now on named B2-A (first 50 years period from IPCC B2 run) and A2-A (first 50 years period from IPCC A2 run); and from the years 2050 to 2099, from now on named B2-B (second 50 years period from IPCC B2 run) and A2-B (second 50 years period from IPCC B2 run).

Three different model levels were analyzed from the ocean output in this study. Level 01 (L01) at depth of 12.5603 m, considered a surface level; Level 04 (L04) at a

depth of 90.2559 m, to represent an estimate of the average thermocline depth in the Eastern Pacific; and Level 08 (L08) at a depth of 211.587 m, to represent an estimate of the average thermocline depth in the Western Pacific. We must mention that an attempt of calculating a thermocline depth was made, but it was not successful due to the fact that the PCM does not have sufficient levels in the top 300 m of the ocean (only 10 levels, Meehl et al., 2001), that are too spaced to calculated a thermocline depth by interpolation methods. In addition, we consider important to maintain the characteristics of the model as invariable as possible, meaning that we selected to keep the grid of the model in its original form, by not forcing a higher resolution in the first 300 m of the model by some sort of interpolation.

OTA indices were calculated from six different regions (two in the Equatorial Pacific and four along the west coast of South America), to examine the possible variation of the ocean-atmosphere dynamics under the GHS future scenarios. Each of the indices was calculated as the mean SSTA over each selected region averaged over time. Similar methodologies have been used by van Oldenborgh et al. (2005) in a multi-model study to examine the response of zonal wind stress to different locations of SST anomalies along the Equatorial Pacific and by Hoerling et al. (2001) to observe the sensitivity of the surface climate in North America under different positions of SST anomalies along the Equatorial Pacific.

The areas in the Equatorial Pacific for the calculating the indices were the Nino 3.4 region (N34, 5° S - 5° N, 170° W - 120° W), extensively used as indicator of ENSO, the Cold Tongue Index (CTI, 5° S - 5° N, 170° W - 120° W), characterizing the cold SSTs (typically < 26° C) in a narrow latitudinal band centered on the equator in the central and eastern longitudes of the Pacific basin (Deser and Wallace 1990).

Along the coast of South America, the election of the different regions was based on the study done by Montecinos et al. (2003) where they investigate the relation of SST of nine stations along the west coast of South America and global SST in the period 1951-1999. They showed that ENSO-related SST variability decreases poleward from subtropical latitudes, while interdecadal variability increases from subtropical to mid-latitudes, in agreement with similar results along the western coast of North America. In this study three regions with well define different patterns of response are evident; these regions also coincide with known oceanographic, atmospheric and geographic changes along the coast and with a different distribution of the species that support the fisheries. Based on this areas of response we select the following regions, named as South America 1 (SA1, 10° N - 5° S, 90° W - 77° W); South America 2 (SA2, 5° S - 21° S, 90° W - 68° W), South America 3 (SA3, 21° S - 38° N, 90° W - 68° W), South America 4 (38° S - 55° N, 90° W - 68° W). Notice that the region SA1 includes a small area of the Caribbean Sea and region SA4 includes a small fraction of the south West Atlantic; those areas were not taken in consideration for the calculation of the indices (Figure 1).

With the intention of removing the global warming trend and being able to recognize future changes in the ocean features under GHG forcing, an EOF analysis, weighted by area, was performed on the 50 years periods of OTA for the future IPCC runs (B2-A, B2-B, A2-A and A2-B). Weighting the EOF analysis by the area of the POP grid prevents over representing regions on the EOFs (spatial pattern) due to particularities of the POP grid (for example on weighted EOFS, see Wilks, 2006 pp.479, Emery & Thomson, 2004 pp. 341, Santer et al., 1995). In addition, similar EOF analysis was done to the OTAs of the CTRL and the HIST ensembles.

A linear least-squares fit was computed from the first PC for the IPCC runs, CTRL and HIST. To eliminate the warming trend from the SSTA, the calculated linear fit

was multiplied by the first EOF to create a warming trend spatial pattern over time, which then was subtracted from the corresponding OTA of the IPCC runs, CTRL and HIST ensembles.

Linear correlations maps were computed between the seasonal indices (N34, CTI, SA1, SA2, SA3 & SA4) and the analogous seasonal OTA at the different model levels for each 50 years period (CTRL, HIST, B2-A, B2-B, A2-A, A2-B). The p-value for each correlation map was also calculated to show the significance of the correlations at 95 % confidence level.

Correlation differences maps were computed to look for possible modifications in the spatial relationships between the indices and the OTA under GHG forcing. The correlations difference maps were calculated by subtracting the future runs (A2-A, A2-B, B2-A and B2-B) from the CTRL and HIST runs.

To confirm the significance of the difference maps, a null hypothesis test for the difference between two correlations coefficients was performed for each of the grid points, using the methodology from Cohen et al. (2003). (For a straightforward description on the null hypothesis test the difference between two correlations coefficients refer to: http://www.fon.hum.uva.nl/Service/Statistics/Two_Correlations.html).

For the analysis and interpretation of the results, we must consider that linear correlations coefficients are neither robust nor resistant. They are not robust because strong non-linear relationships between the variables X (in this case, OTA) and Y (the indices) may not be recognized.

To investigate the changes in ENSO statistics and their propagation into the SEP, we calculated the frequency distribution of OTA for the seasonal indices (N34, CTI, SA1, SA2, SA3 & SA4) for JFM and JAS.

After removing the warming trend (by the previous mentioned methodology), we produced OTAs climatologies and standard deviation differences maps between the future runs and the CTRL and HIST. For those differences maps, a T-test was computed to illustrate the significant different regions with 95 % confidence (von Storch and Zwiers, 1999). This calculation was done with the intention of enhance the regions with major temperature changes under GHG forcing.

Finally to compare the PCM ocean outputs with observations, we used the UK Meteorological Office, Hadley Centre HadISST data set version 1.1 (British Atmospheric Data Centre 2006). This data set contains global monthly SST climatologies from 1870 to the present, with 1° by 1° resolution. We subsample two periods, from 1900 to 1949 and from 1950 to 1999, with the intention of having 50 years of data to compare with the PCM SST. SSTA were calculated for this data set (HADSSTA) following the same methodologies mention above. To remove the long term trend a weighted EOF was calculated with the same approach as for the PCM OTA. Similar indices (CTI, N34, SA1, SA2, SA3 and SA4) were calculated for the HADSSTA with the objective of creating correlation maps and correlation maps differences between the two HADSSTA periods (1950-99 minus 1900-49) to investigate if similar “ENSO-like” patters will emerge in the observations.

CHAPTER 4

RESULTS

4.1. Analysis and Results

The analyses of OTA EOFs illustrate the spatial pattern of the SSTA warming trend as a result of a change in the Earth's energy balance due to an increase in GHG. Figure 2 displays the EOF patterns for SSTAs smoothed with a double 5-month running-mean filter to emphasize interannual and lower frequency variability for JFM seasonal averages of PCM ocean output. For the CTRL scenario the main pattern is ENSO, while in the HIST ensemble the warming trend starts to become evident. On the B2-A and A2-A EOF maps the warming trend is more observable not only along the equator but expanding through the tropics and sub-tropics with enhanced warming over the Gulf of Alaska. For the B2-B and A2-B EOF maps, the warming trend has spread across the Pacific Ocean; however in the A2-B EOF the warming is more uniform, whereas in the B2-B EOF map the warming trend has structures that resemble a warm (positive) PDO pattern (Mantua & Hare 2002). In addition, on this map, the warming in the SEP is confined to several hundred km off the coast, following an "ENSO-like" type of pattern. It is interesting to compare the JFM EOF maps with the JAS EOF patterns (not shown). They share similar spatial features but the JAS EOFs have a more intense warming with higher variance explained by those patterns. In the B2-B EOF for the JAS seasonal average, the PDO pattern is less evident and the coastal warming of the SEP expands farther offshore.

For the PC analysis in Figure 3, representing the time series of the EOFs in Figures 2, there is distinguishable warming trend in the HIST ensemble and IPCC scenarios B2-A, A2-A, B2-B and A2-B. There are similar tendencies for the PC analysis of the JAS seasonal averages (not shown).

When looking into the HADISSTA EOF maps (Figure 4), we observe a warming trend during the period from 1900 to 1949 for both seasonal averages (JFM and JAS), which is reflected in the corresponding PCs (Figure 5). Observe that the warming trend represents approximately 50 % of the total variance for this era. Similarly, for the period from 1950 to 1999 for JFM and JAS seasonal averages, a sharp warming is evident, with a spatial pattern resembling the warm (positive) phase of the PDO. The PCs corresponding to the same period reveal a linear warming trend with a slightly gentle slope, if compared with the PCM PCs (Figure 3) from the HIST ensemble and the future B2 and A2 scenarios. In the HADISSTA PCs for the period 1950-1999, the warming on the SEP is restricted to several hundred km off the coast, in accordance with an “ENSO-like” pattern.

Previous studies looking into ENSO statistics in GHG forced scenarios did not find major changes, but in our analysis of the PCM OTAs we found an increase in the SSTA amplitudes (larger ENSO events) based on inspection of the frequency distributions of SSTA (Figure 6) for all the indices we created (N34, CTI, SA1, SA2, SA3 & SA4) for both seasons (JFM and JAS). In all areas that were studied, the distributions of SSTAs for the CTRL and HIST ensembles SSTAs are highly clustered between –0.5° to +0.5° C, with a higher occurrence of colder events For the N34 Index (Figure 6, top six plots), 82 % and 90 % of the frequency distribution occurs between –0.5° to 0.5° C for the CTRL and HIST ensembles, respectively. The structure of these frequency distributions becomes narrower for regions further southward along the SEP coast. For

example, the SA3 Index frequency distribution (Figure 6, bottom six plots) has 100 % of the SSTA for the CTRL and HIST ensembles over the same range (+-.5). Under the future scenarios the spread of the SSTA anomalies ranges to -1.25° to 1.25° C along the equator (CTI, N34 and SA1) with a higher number of colder events than warmer events. In the SA2, SA3 and SA4 regions, the widening of the distribution progresses into a –1.25° to 0.75° C span, indicative of the narrowing of the overall distribution with distance southward of the equator. In a GHG-warmed world, the N34 Index frequency distribution within the –0.5° to 0.5° C range is reduced to 88% (B2-A), 66% (B2-B), 66% (A2-A) and 80% (A2-B) of the total and the frequency distribution for the SA3 index within the same anomalies range is reduced to 98% for all future scenarios. This illustrates a small tendency towards stronger ENSO events (EN and LN) under GHG forcing in these simulations. In the real world, however, the changes in the frequency of ENSO will depend on future GHG forcing conditions, as we can observe from the different results that occur here for different IPCC scenarios. We will address the issue of a higher number of colder events in the PCM in the discussions section.

While looking into the ENSO statistics in the HADISST data set, we found that there is an increase in the amplitude of the SSTA for all the created indices when comparing the SSTA from 1900-1949 versus 1950-1999. This tendency for larger amplitude ENSOs with time is generally consistent with the results found for increasing GHG in the PCM, though not specifically for those time periods. In the observations, there is mainly an amplitude increase towards warmer events for all indices, but there are areas (N34, SA1, SA3) in which there is also an increase in the number of extreme cold events (Figure 7).

Correlations between SSTAs and regional indices serve to quantify the strength of the ENSO teleconnections and can be used to assess the differences between the

periods of the future IPCC runs and the CTRL / HIST ensembles. We are especially interested in investigating the changes in teleconnections between the Equatorial Pacific and the SEP. Figure 8 represents a schematic of how those maps were obtained. Our hypothesis of a poleward expansion of the ENSO teleconnections in a GHG-warmed world will be reflected as a change in the spatial structure of significant correlations bearing an “ENSO-like” pattern.

A remarkable pattern occurs in the maps of correlation differences. The changes in the correlations are not focused along the Equator. Instead, the changes are more prominent off the Equatorial region, especially in the subtropical and extratropical regions (Figures 9 and 10). Previously published results about ENSO statistics in a GHG-warmed world (Collins et al. 2005, van Oldenborgh et al. 2005), revealed that no major changes in ENSO statistics occur. But those results were mostly based on focusing on the equatorial region, which is consistent with our results of little change in the teleconnection patterns along the Equator. But our results reveal that significant changes in teleconnection patterns do occur, under increased GHG forcing, in regions off the equator along the coasts of South and North America.

Another important finding from the maps of correlation differences is that the changes in the correlation patterns are scenario-dependent and period-dependent, even after removing the warming trend for each period. The differences in correlation generated by the IPCC B2 scenario tend to be markedly spread poleward compared to the differences generated by the IPCC A2 scenario. In addition, the A2 scenario differences in correlations tend to be more intense and localized in specific regions. When comparing the two future periods of each IPCC scenario (2000-2049: B2-A, A2-A and 2050-2099: B2-B, A2-B) with the CTRL and HIST ensembles, we found that the

most intense changes in correlations are produced during the first period (2000-2049) for reasons that are not clear.

The correlation differences with the N34 index show an increase in correlation under the two future IPCC scenarios for an area starting from the central-southern coast of Chile extending into the Central Equatorial Pacific with a southeast–northwest tilt. However, under the IPCC B2 scenario the increase in correlation gives the impression of being more coastal and localized, even with a poleward expansion to the Southern Ocean under the B2-A period compared to both the CTRL and HIST ensembles, and a weaker positive difference in the B2-B period. At the same time, the N34 index and SSTA correlation differences for the A2 have the same region of increased correlation, but with a more pronounced southeast–northwest tilt, no expansion toward the Southern Ocean and higher positive values than the B2 case (top four plots in Figures 9 and 10). In addition, the differences with the HIST ensemble show for both IPCC scenarios a slight increase in correlation right off the Equator, immediately followed by poleward asymmetric areas of decreased correlations with noteworthy values. In the North Pacific, an important region of decreased correlation is evident for the differences of both future IPCC scenarios with the HIST ensemble, appearing to suggest a decrease in the teleconnections between the Equatorial Pacific and the Pacific Decadal Oscillation (PDO) (Schneider and Cornuelle, 2006). It is important to mention the noticeable increase in correlations for the A2-A / HIST difference in a significant area from the West Coast of the United States and Baja California extending into the Central Equatorial Pacific with a northeast–southwest tilt. All these areas with increased correlation for the N34 index illustrate a poleward expansion of the “horseshoe shape” of the interannual ENSO pattern, by highlighting (via increased correlations) the poleward broadening of the edges of the horseshoe shape.

For the SA2 differences in correlations, the region of increased correlations off southern-central Chile is present under both future IPCC scenarios; however the correlation differences are less intense for both periods in comparison with the N34 differences (central four plots in Figures 9 and 10). Only for the IPCC B2-A scenario, the entire Equatorial Pacific region develops a reduced correlation with SA2, suggesting a decoupling of this region from ENSO processes in this case. The SA2 region also has a reduction in correlation with the PDO teleconnections of the North Pacific, especially during the 2050-2099 period, for both IPCC scenarios. The area of increased correlations from the West Coast of the United States and Baja California towards the Central Equatorial Pacific seen in the N34 correlation pattern change for the A2-A / HIST differences is also present in the SA2 index but with less intensity.

The differences between results for each IPCC case and time interval tend to be more evident further from the equator, indicative of the tropical ENSO effects being the dominant driver of the teleconnections, even for the indices associated with the west coast of Peru and Chile (S2, S3 and S4; central and bottom four plots in Figures 9 and 10). For the IPCC B2 scenario, the SA4 index exhibits a major increase in correlation for both periods with an “ENSO-like” spatial pattern, again suggesting dominant control of this region by ENSO processes. The 2000-2049 period again has higher positive values of the difference in correlations, spreading continuously from the SEP coast toward the Central Equatorial Pacific. Interestingly, in both future periods, an elevated positive increase in correlation is evident for the area between the United States coast and the Central Equatorial Pacific, extending farther north to Canada and the Gulf of Alaska, but not covering Baja California. This suggests stronger contemporaneous response of the eastern boundary current systems of the North and South Pacific to ENSO forcing in this scenario. The anti-correlation of SA4 with the central North Pacific PDO type pattern

increases as well. For the IPCC A2 scenario, the changes in correlations for SA4 are generally consistent with those found in the B2 case. The increased correlation with the Equatorial Pacific are now weaker, but the strong positive increase along the North Pacific eastern boundary occurs as the most prominent change in this case as well. In contrast to B2, for the differences with the CTRL ensemble, the Equatorial Pacific positive increases in correlation are the core pattern. For the HIST ensemble differences, the increase in correlations in the Equatorial Pacific is limited to the region west of 160° W. In addition, there is a higher increase in correlation for the Northern Pacific than the Southern Pacific during the 2050-2099 period. The decrease in correlations is mostly restricted to the West Pacific with an almost symmetrical distribution across the Equator during the 2000-2049 period, but with a stronger and wider signal in the North Pacific. For the 2050-2099 period, the North Pacific PDO type pattern intensifies suggesting a stronger influence of the PDO (as previously found with other indices). Although the South Pacific changes are much weaker, they still exhibit the poleward broadening of the ENSO impacts found for case B2.

4.2. Possible Effects on the HCE

On the coasts of Peru and Chile, humans have had a close relationship with the ocean for thousands of years, depending on it as an important source of their daily diet. The oldest known archeological sites along the coast of Peru are 12,000 to 14,000 years old and the oldest fishing net known to be made by the Peruvian pre-Columbian Paracas culture is 9,000 years old (Buse 1975, Wust 2006). Since their early contact with the ocean, fishermen along the SEP have learned to understand the association of marine species with oceanographic and atmospheric phenomena. Nowadays, popular

knowledge has grown into relating warm and cold events with abundance or disappearance of certain species, such as high concentrations of anchovies in colder events, and high abundance of sardines, mackerel and jack mackerel in warm events. There have been numerous scientific publications about the effects of oceanographic conditions of the SEP on marine fauna and flora, emphasizing the influence of climatic change at different temporal scales, such as EN and LN events, and regime shifts (Fiedler 2002, Bakun and Broad 2003, Chavez et al. 2003, Alheit and Niquen 2004, Bertrand et al. 2004, Escribano et al. 2004, Niquen and Bouchon 2004).

From our EOF maps of the SSTA in the PCM output (Figure 2), we observe an “EN-like” warming pattern along the SEP coast under both IPPC scenarios, with the warming trend increasing with time (Figure 3). These circumstances could have serious consequences for the recovery of the anchovy and sardines populations after an EN event in the HCE. Anchovies and sardines control the trophic dynamics of upwelling systems (Cury et al., 2000), and are normally constantly exploited by industrial and artisanal fisheries (Carr and Broad 2000, Bakun and Broad 2003). The size of the biomass for these species closely depends on the previous year-classes (one year for anchovy and three years for sardine), due to the short lifespan of the fish and their heavy exploitation (Brochier et al. 2008). In general for small pelagics, it is accepted that recruitment depends principally on survival during the first life stages rather than in the spawning biomass, and the achievement of good survival rates is largely ruled by environmental conditions (Bakun 1996). Anchovy eggs off Peru require temperatures around 16 °C for about 2 days to develop, similar to the mid-range of temperatures observed in situ during the spawning season (Santander 1987). Food availability and type are also very important factors for larvae survival (Castro et al. 2000). Therefore, higher temperatures as a result of a GHG-warmed world, and its impact on local

phytoplankton, could have a direct impact on recruitment success, which will translate rapidly into fluctuations in population biomass.

Generally, during an EN event anchovies adapt to the warming conditions by finding small-scale 'loopholes', or areas where the oceanographic conditions are favorable for their survival during the warm event (Bakun and Broad 2003, Bertrand et al. 2004). During the early stages of EN, the persistence of local coastal "efficient" upwelling (Barber and Chavez 1983) provides shallow inshore pockets of cold water where anchovy is concentrated (Bertrand et al. 2004). In addition, there is a southward migration, and deepening of the schools to approximately 150 m, out of reach of the purseiner fishing nets (Gutierrez 2001, Gutierrez et al. 2007). After EN, conditions progressively return to "normal" or develop into LN events, allowing a rapid stock recovery of the anchovies, mainly due to favorable conditions for the newly recruited population and the adults that survive the event (Niquen and Bouchon 2004). However, if the conditions do not return rapidly to "normal" temperatures due to warming forced by GHG, the recovery of the population may be dangerously affected because temperature anomalies and food supply play important roles in Peruvian anchovy growth and population dynamics. The combination of both changes in temperature anomalies and food supply in a GHG-warmed world may magnify the impacts of EN on the anchovy stocks in the HCE. There is an ongoing scientific discussion about if a the anchovies will migrated poleward or stay in more coastal waters as a result of the increase in the upwelling due to land-ocean thermal differences (Bakun 1990, Bakun and Broad, 2003). Our suggestion is that the recruitment could be seriously affected under a strong ENSO event under an "El Niño-like state" (see also Niquen and Bouchon 2004).

Figures 6 and 7 show an increase in the amplitude of SSTA along the Equator and the coast of the SEP under future IPCC scenarios and observations. During EN

events, there is a pronounced change in the vertical and latitudinal distribution, with a displacement from north to south and west to east, of several marine species. This displacement can be viewed as the shift of a system with its integral species, as the thermal anomaly is intensified. The intrusion of warm waters from the tropical Pacific to the HCE during the EN events has promoted transient suitable areas for tropical species that could diversify the food supply for local predators all across the marine food chain, representing a tropicalization of the HCE (Arntz and Fahrbach 1996). Resident species like anchovy become patchier and asymmetrically distributed towards the southern Peruvian coast, instead of being widely distributed over the whole Peruvian coast as in "normal" or LN conditions. Sardine shoals also were displaced from the north-central to the south-central area (Bouchon et al. 2000, Niquen and Bouchon 2004). There were also considerable changes in the size structure in anchovy during EN 1972-73, 1982-83 and 1997-98. Adult fish were predominant and young fish were generally few or absent, which impact recovery and population growth. The biomass of juvenile sardines and other fish increased during EN.

Figures 8 and 9 shows a poleward expansion of ENSO teleconnections under GHG forcing by means of a poleward increase of SSTA correlations between the SEP coast and the Equatorial Pacific, with an "ENSO-like" correlation pattern. These results support the possible changes on the vertical and latitudinal distribution of marine species, changes in the size structure of pelagic fish, and the tropicalization of the HCE as a consequence of an expanded ENSO teleconnection in a GHG-warmed world. Niquen and Bouchon (2004) stated: "If the conditions are warm, the change will be long lasting, and if the environment is cold, other pelagics will tend to disappear, originating a rapid return of anchovy".

A primary caveat for these responses of the HCE marine species to transient EL Nino events in a GHG warmed world is the theory proposed by Bakun (1990) in which GHG forcing produces warmer surface air temperatures over land relative to those over the ocean, generating an increase in upwelling-favorable winds in response to strengthened land-sea thermal contrast and land-sea-atmosphere feedbacks. He showed an augmentation of alongshore wind stress in several regions of the world since the mid twentieth century. Similar results were obtained with paleoceanographic data by studies presenting an increase in coastal upwelling along Northwest Africa (McGregor et al 2007), California Current (Field et al. 2006), and arid region of southern Peru and northern Chile (Vargas et al. 2007). If this is the case, the HCE coastal regions will generate colder, more favorable background conditions for anchovies, and create intense sharp fronts dividing the upwelled cold waters and the GHG-warmed off shore waters.

In order to understand the real effects of global warming and altered ENSO characteristics on marine species and the economical activities that they support, it is necessary to generate high-resolution GHG-forced coupled models that could resolve submesoscale processes, which play important roles on the marine biological dynamics.

4.3. Concluding Remarks

In terms of scientific inputs, industrial fisheries are generally perceived as local interactions necessitating annual reassessments of species-specific catch quota, managed to directly benefit the fishers themselves. Most fisheries scientists are employed by regulatory government institutions that generate these quotas, which ideally should make fisheries sustainable and profitable, contributors to employment and, through international trade, to global food security. Under this fisheries panorama,

neither global predictions, nor the collaborative development of long-term scenarios are normally included in the managing scenarios. In recent years, the view of fisheries production and management has changed into having a global perspective, on its way to managing its supporting ecosystems. With this study we intend to contribute to this global view with an assessment of possible effects of global warming in one of the most productive fisheries region in the world, the HCE, with the goal that the fishing industry and its management institutions incorporate mitigating strategies for a GHG-warmed world.

We identify the warming trend spatial patterns in the Pacific Ocean with special focus on the SEP. The intensity and structure of those patterns are dependent on the future IPCC scenarios. An augmentation of the amplitude of the interannual SSTA in the Nino 3.4 region and along the coast of the SEP was found in the PCM IPCC runs, and we corroborated those results with observations from the HADISST data set.

We show that ENSO teleconnections under GHG forcing could have a poleward expansion as a consequence of changes of the atmospheric circulation, resulting from a variation of the background into an “ENSO-like” condition. Vecchi et al. (2006) show with observations and models a reduction of the Walker Cell atmospheric circulation, consequently altering the thermal structure and circulation of the tropical Pacific Ocean. Furthermore, Vecchi & Soden (2007) illustrate a general weakening in the atmospheric circulation due to a reduction of the frequency of strong updrafts and increasing the frequency of weak updrafts. This translates into a preferential reduction the Walker cell (zonally asymmetric atmospheric circulation) rather than Hadley Cell (zonal-mean) component of the tropical circulation (see their figure 7), generating significant changes to the thermal structure and circulation of the Pacific Ocean, which look a lot like “El Niño–like” conditions, but with different mechanisms to those from EN events. Our

results support Vecchi and Soden (2007) conclusions, by showing a latitudinally and poleward expansion of atmospherically forced ENSO teleconnections influenced by the “ENSO-like” warming trend of the ocean-atmosphere background state as a result of GHG forcing.

The impacts of those changes are visible on the SSTA all along the coast of the SEP, with more substantial impacts in central-southern Chile than in Peru. These GHG-forced changes in ENSO anomalies could translate into a possible tropicalization of the HCE, vertical and latitudinal distribution changes of marine species, and changes in the size structure of pelagic fish, which could have a dramatic impact on the economical activities that depend on the normally very productive HCE.

FIGURES

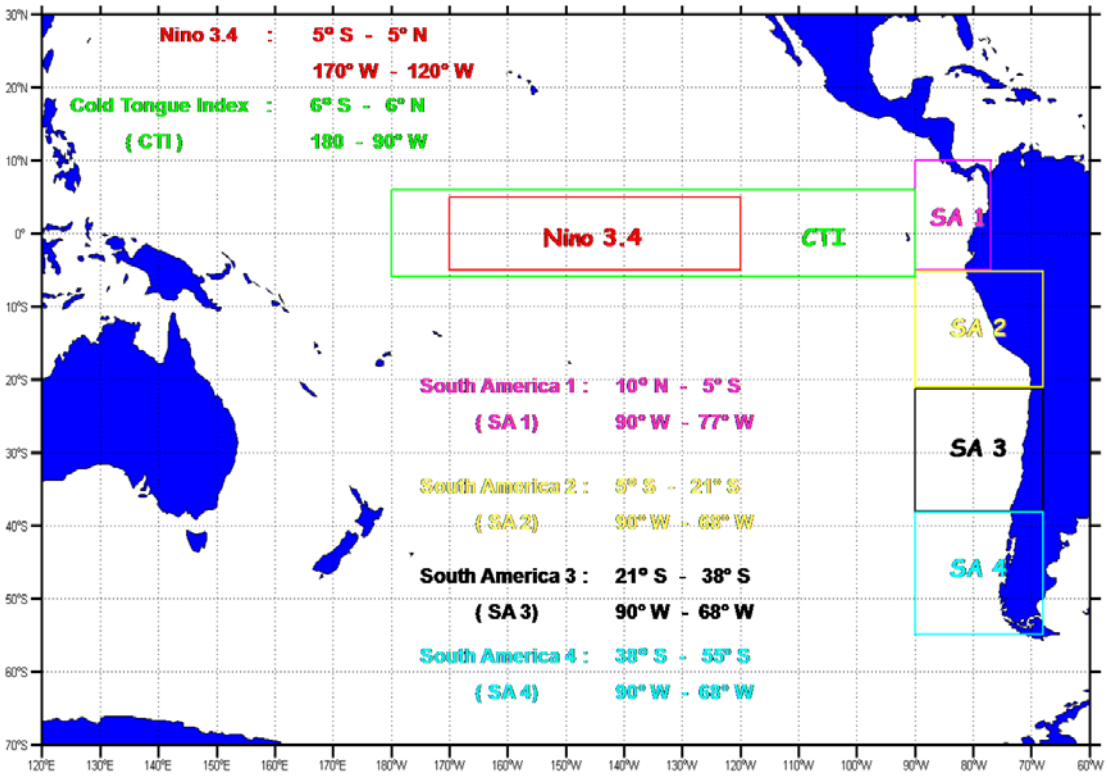

Figure 1. Map locating the indices, with respective coordinates, used for creating the correlation maps with OTAs for the Pacific Ocean of the PCM ocean outputs.

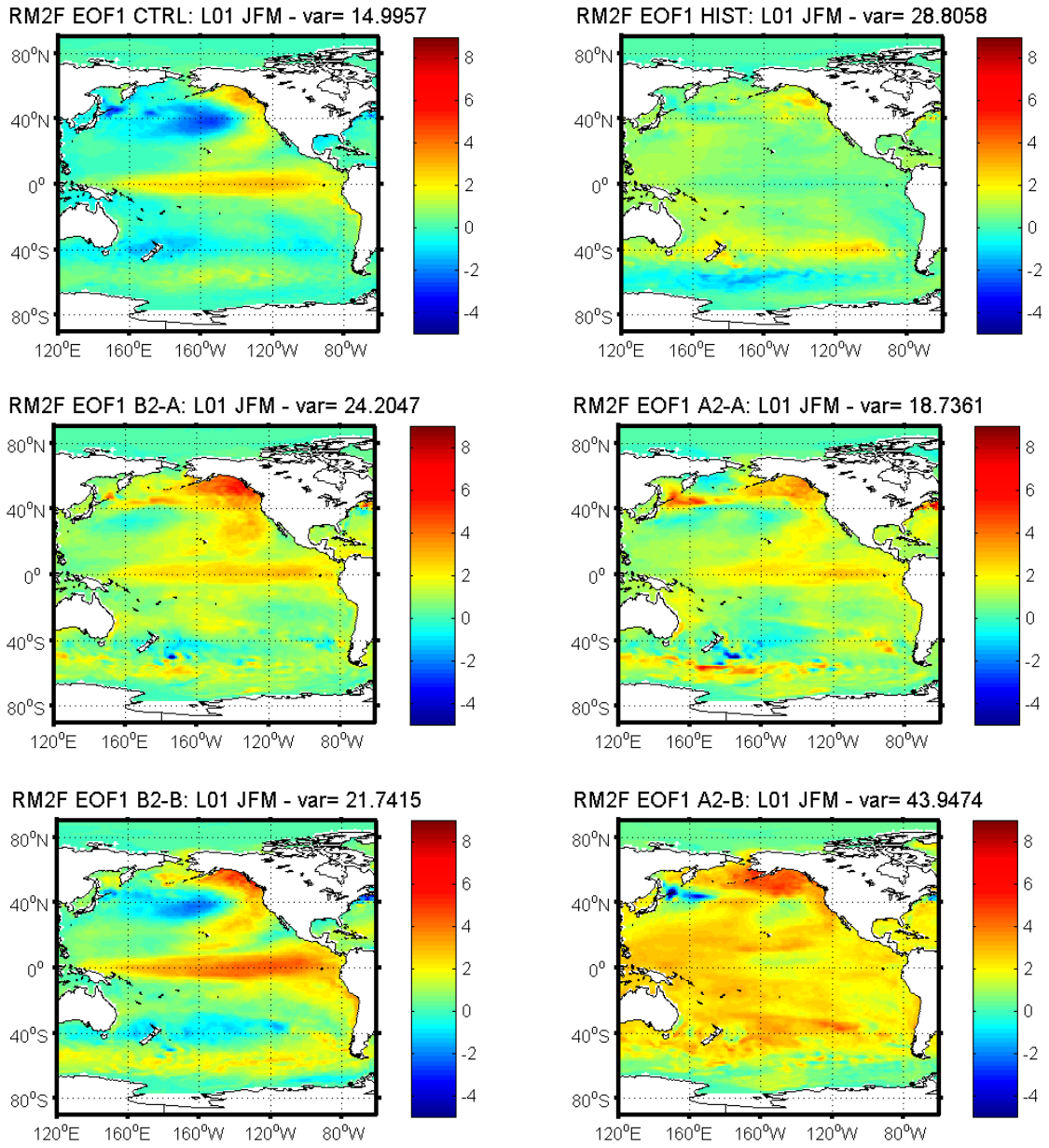

Figure 2. First EOF SSTA smoothed with a double 5-month running-mean filter to emphasize interannual variability for January, February and March (JFM) seasonal average of PCM ocean output for CTRL ensemble (top left), HIST ensemble (top right), IPCC B2-A scenario (middle left), IPCC A2-A scenario (middle right), IPCC B2-A scenario (bottom left), IPCC A2-A scenario (bottom right). The variance (var) that first EOF represents is shown on top of each map. Notice how the intensity of the warming trend is more visible in the last 50 years of the future IPCC scenarios.

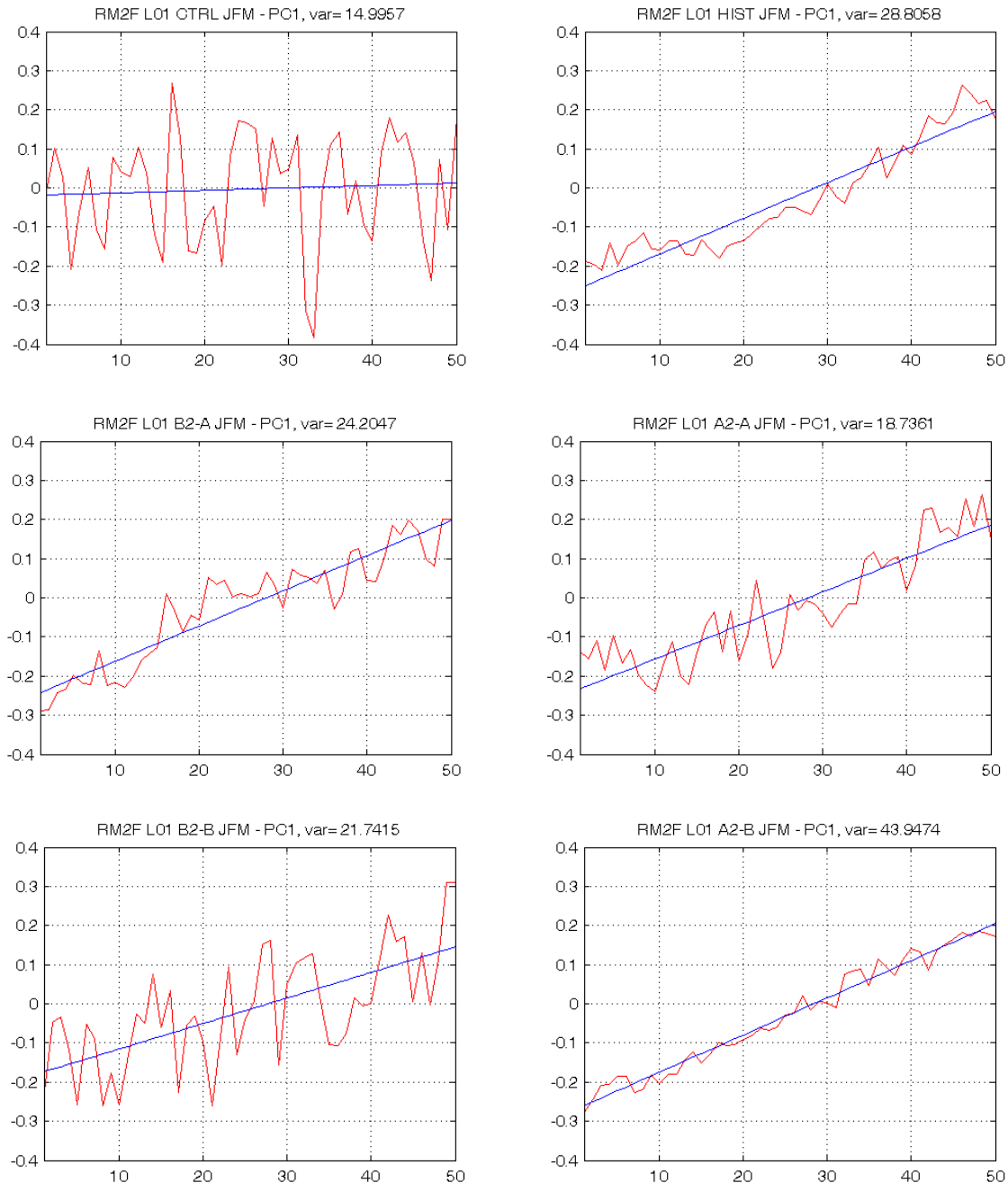

Figure 3. Corresponding first PC (time series) of EOF patterns from Figure 2, for JFM seasonal average of PCM SSTA for CTRL ensemble (top left), HIST ensemble (top right), IPCC B2-A scenario (middle left), IPCC A2-A scenario (middle right), IPCC B2-A scenario (bottom left), IPCC A2-A scenario (bottom right). The variance (var) that the PC represents is shown on top of each map. The warming trend is extremely evident in the HIST ensemble and IPCC future scenarios (B2-A, B2-B, A2-A, A2-B).

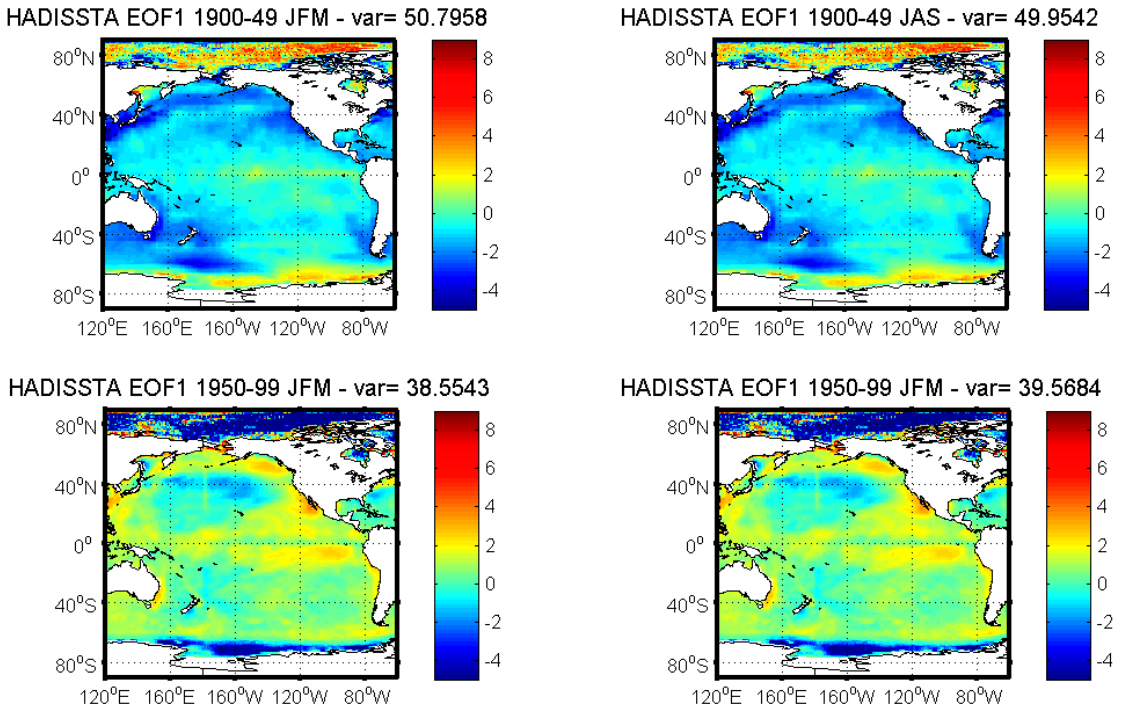

Figure 4. First EOF of SSTA smoothed with a double 5-month running-mean filter to emphasize interannual variability for JFM and JAS seasonal averages of the HadISST data set. The 1900-49 period is on top (JFM on the left and JAS on the right) and the 1950-1999 period at the bottom (JFM on the left and JAS on the right). The variance (var) that first EOF represents is shown on top of each map. A cooling trend is recognizable for the first 50 years period in contrast with the following 50 years period in which a warming trend is evident.

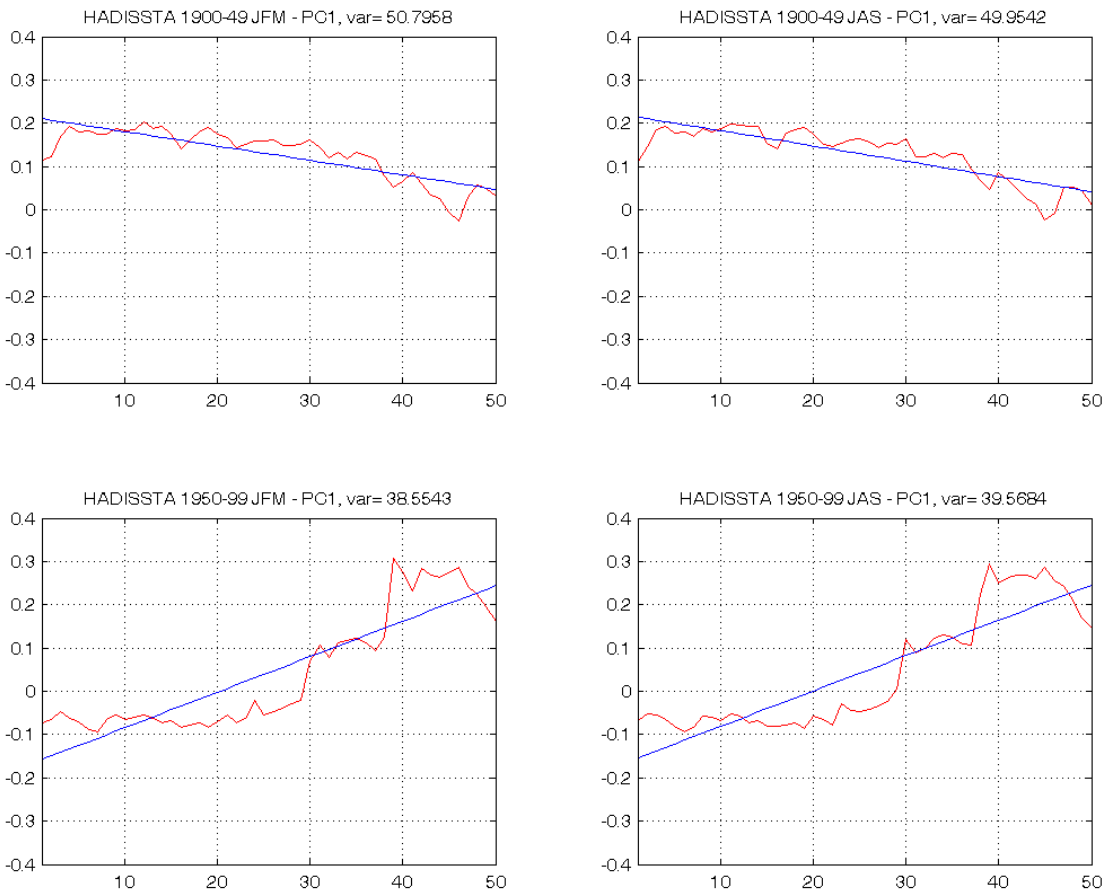

Figure 5. Corresponding first PC (time series) of EOF patterns from Figure 4, for JFM and JAS seasonal averages of the HadISST data set. The 1900-49 period is on top (JFM on the left and JAS on the right) and the 1950-1999 period at the bottom (JFM on the left and JAS on the right). The variance (var) that first EOF represents is shown on top of each map.

Nino 3.4 Index (N34)

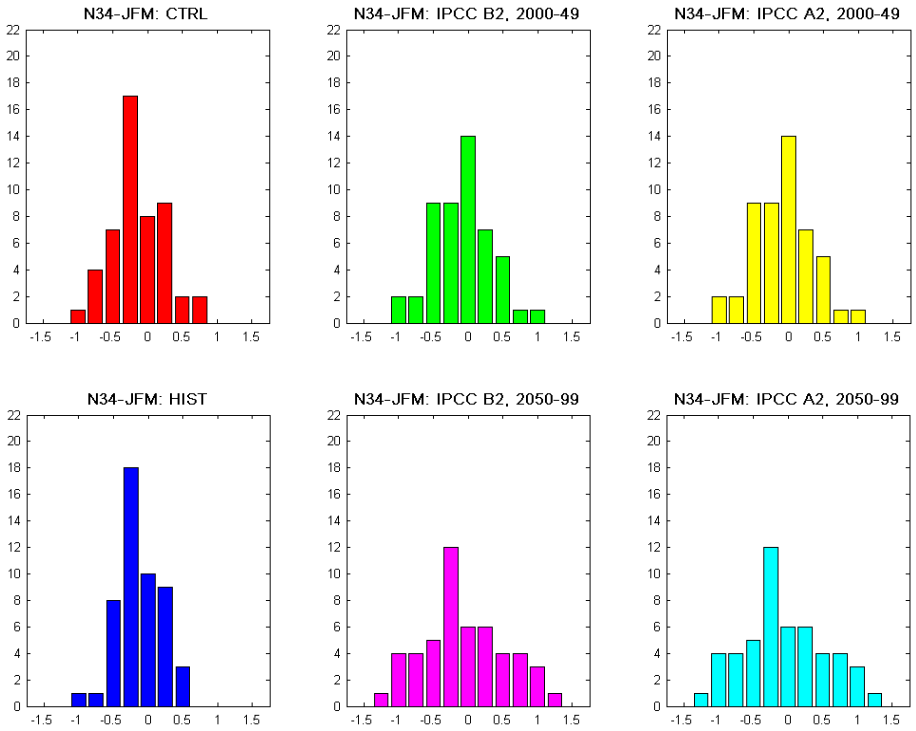

Figure 6. Frequency distribution of SSTA of PCM output for JFM seasonal average of Nino 3.4 Index (top six figures) and South America 3 (bottom six figures) of CTRL (top left) and HIST (bottom left) ensembles, and B2-A (top middle), B2-B (bottom middle), A2-A (top right) and A2-B (bottom right) future scenarios for each of the indices (N34 and SA3). The SSTA were smoothed with a double 5-month running-mean filter to emphasize interannual variability and detrended by their first EOF to remove the warming trend.

South America 3 Index (SA3)

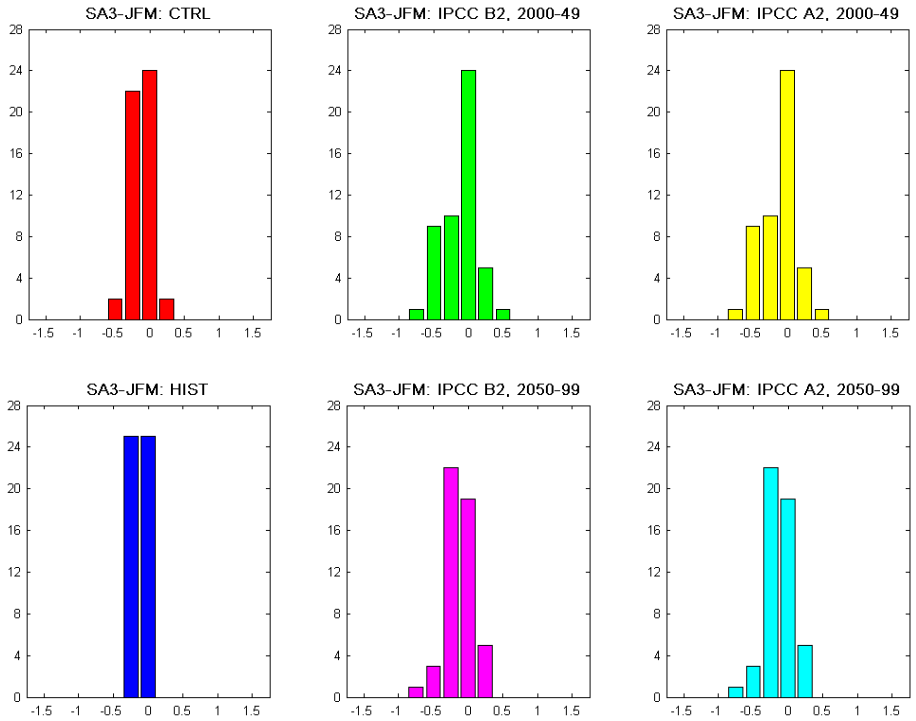

Figure 6. Continued.

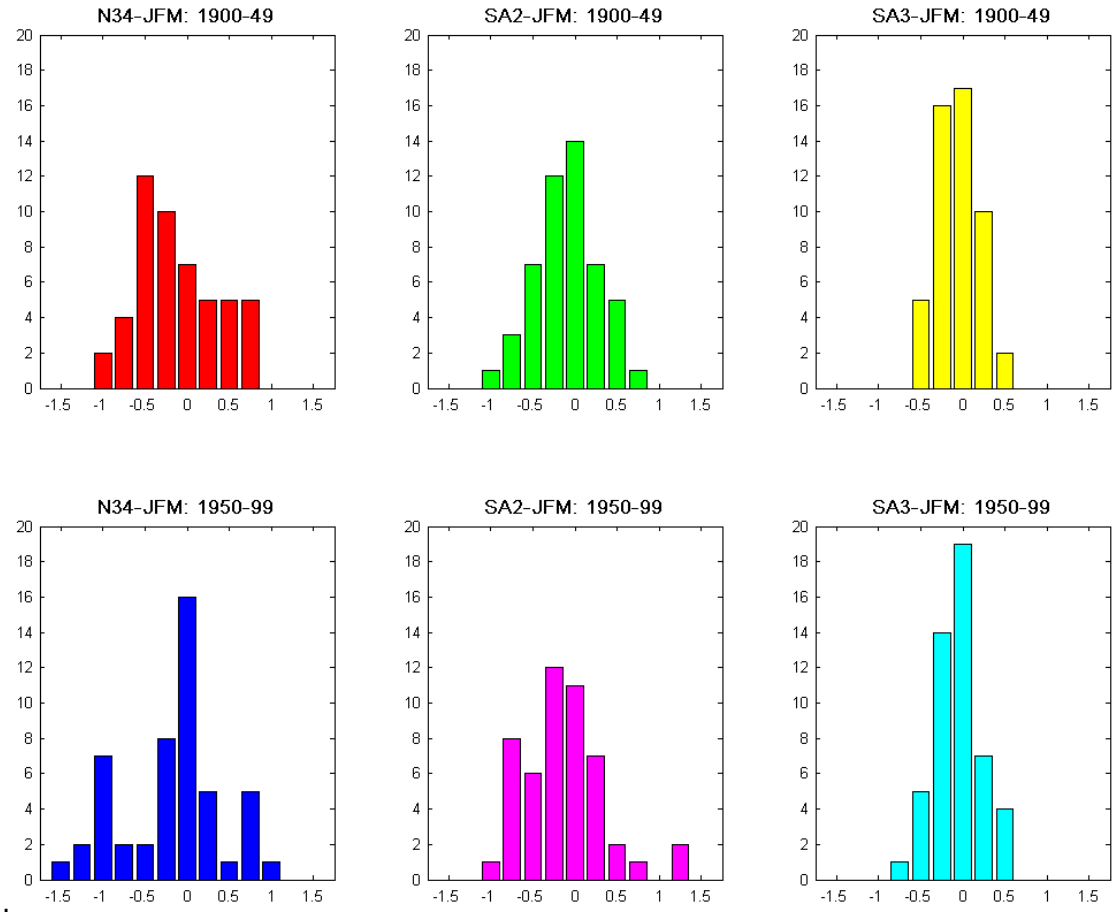

Figure 7. Frequency distribution of SSTA of the HadISST data set for JFM seasonal average of Nino 3.4 Index (right), South America 2 Index (middle) and South America 3 Index (left) for the 1900-1949 (top three figures) and 1950-1999 (bottom three figures) periods. The SSTA were smoothed with a double 5-month running-mean filter to emphasize interannual variability and detrended by their first EOF to remove the warming trend.

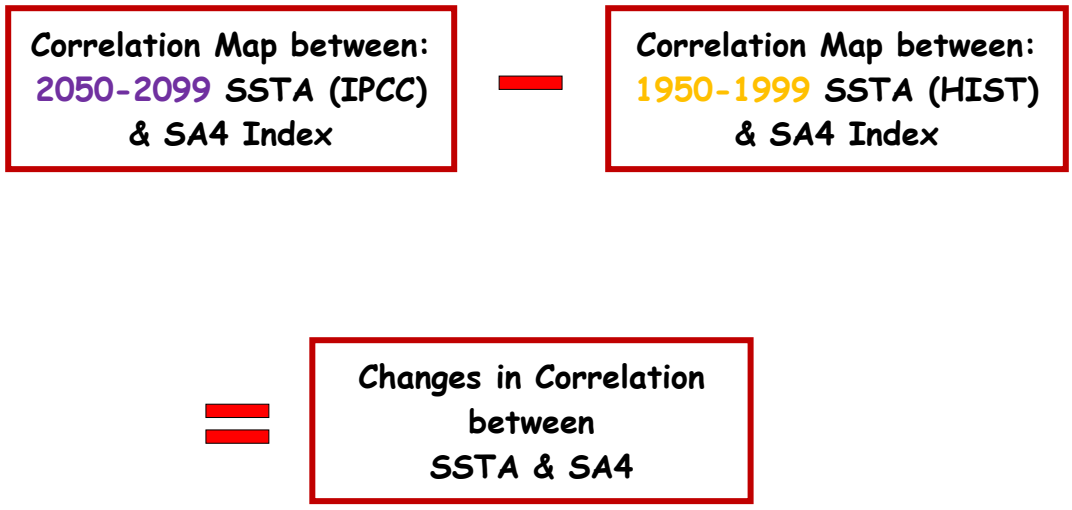

Figure 8. Schematic of the maps of correlations difference. The maps represent changes in correlation by subtracting an IPCC future scenario period (for example, 2050-2099) correlation map of SSTA and one of the indices (for example, SA4) and a correlation map of SSTA with the same index (SA4) of the CTRL or HIST (1950-1999) ensembles. This schematic shows how those differences in correlation maps were obtained.

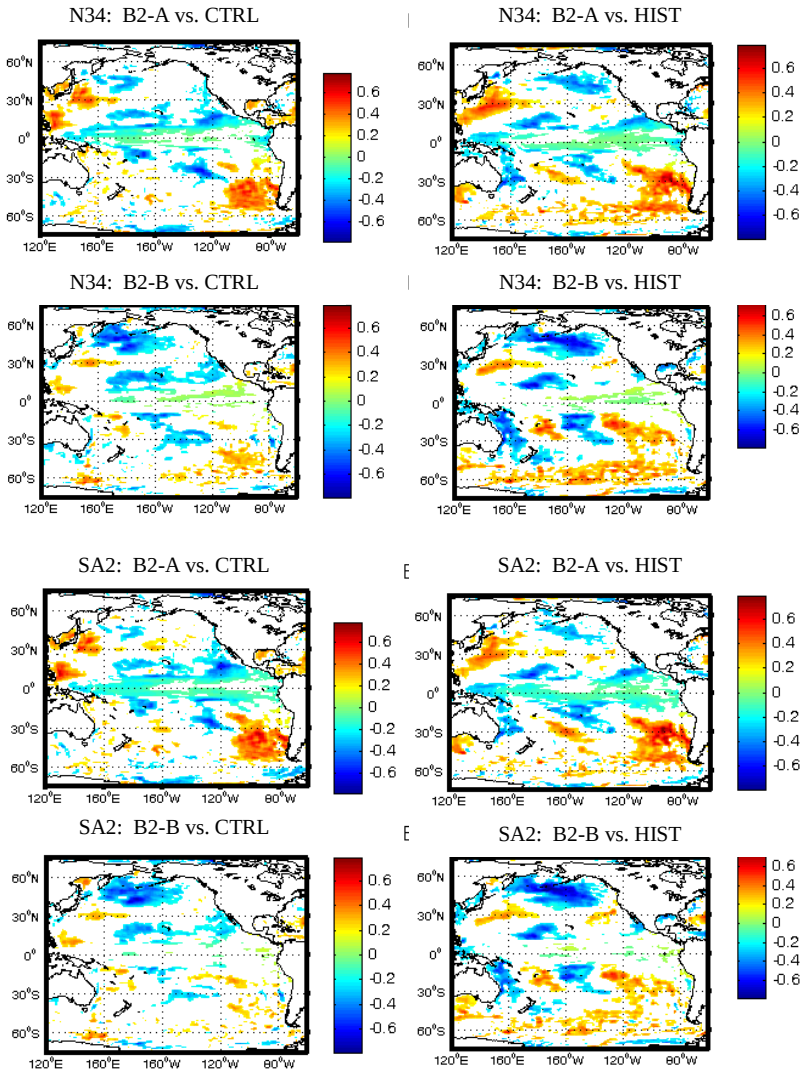

Figure 9. Maps of difference in correlation of SSTA with the N34, SA2 and SA3 indices. The difference in correlation maps were created by subtracting the corresponding SSTA-Index correlation map of the CTRL and HIST ensembles from two periods of the future IPCC B2 scenario (B2-A: 2000 to 2049 and B2-B: 2050-2099). The maps of correlation differences for the N34 index are the top 4 figures, for the SA2 index are the 4 middle figures, and for the SA4 index are the bottom 4 figures.

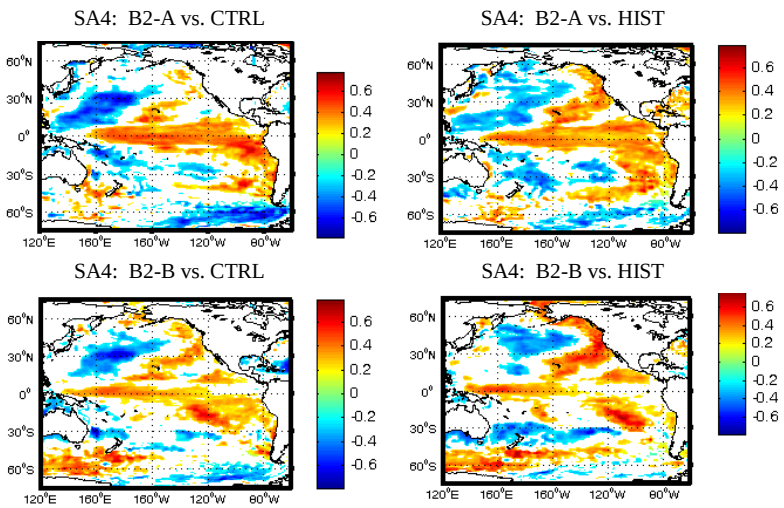

Figure 9. Continued.

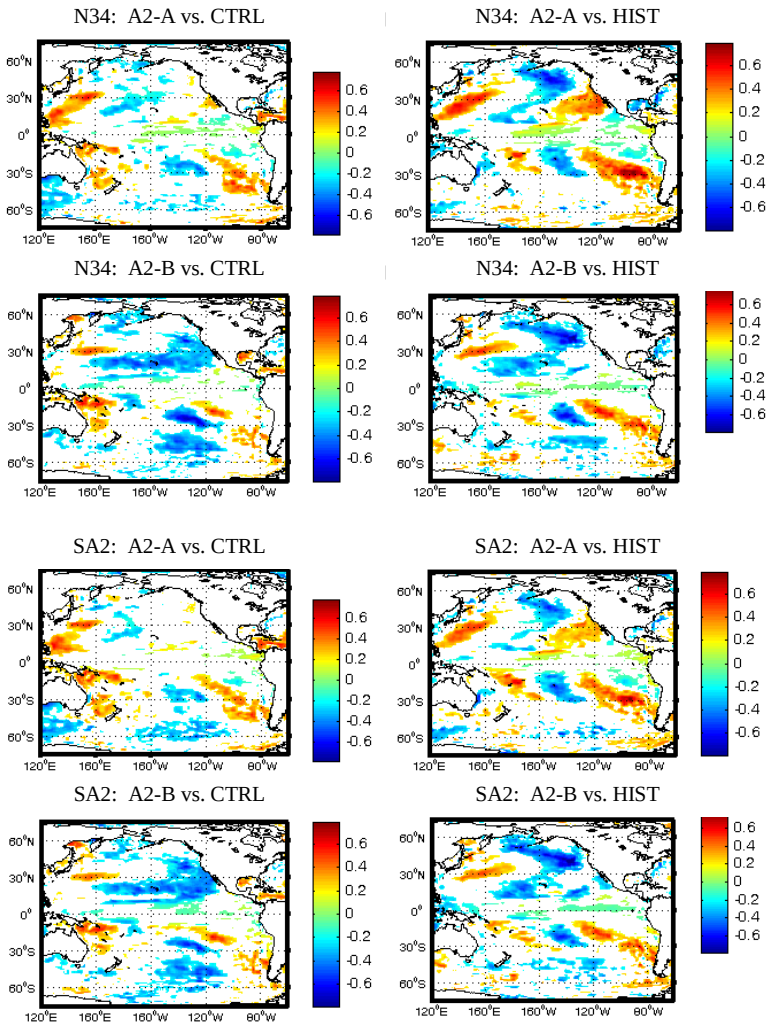

Figure 10. Same as figure 8, but for differences in correlation between the CTRL and HIST ensembles and the future IPCC A2 scenario (A2-A: 2000 to 2049 and A2-B: 2050-2099).

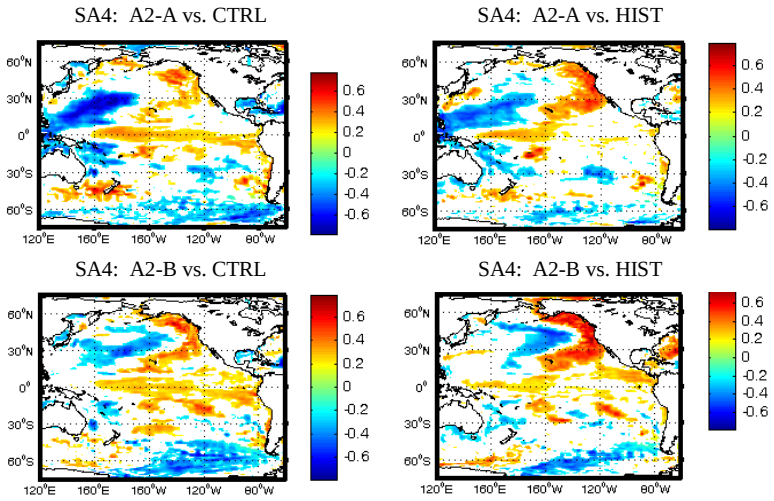

Figure 10. Continued.

APPENDIX

A. OCEAN AND ATMOSPHERIC DYNAMICS OF THE SOUTHERN EAST PACIFIC

The tropical Pacific climatology is characterized by large zonal and meridional asymmetries, with an eastern equatorial “Cold Tongue” (CT) and the Inter-Tropical Convergence Zone (ITCZ), which is mostly situated over the northern tropics. Solar radiation forcing at the top of the atmosphere is zonally uniform and nearly symmetrical about the equator in the annual mean. For this reason, ocean–atmosphere interactions area attributed to the generation and maintenance of these asymmetric features.

The Southern East Pacific (SEP) is characterized by southeasterly trade winds that cross the equator and ITCZ, whose strength varies in response to seasonal variations in insolation, resulting in a pronounced annual cycle in SST (Mitchell and Wallace 1992; Xie 1994). The alongshore wind on the west coast of South America is a major mechanism that keeps the tropical Pacific cool south of the equator (Xie & al. 2007). The winds are associated with a center of high sea level pressure (SLP) anomalies centered around 140° W – 35° S (Garreaud & Battisti 1999). This northward flow is largely confined to the layer below 1 km (Wallace et al. 1989).

The distribution of the SST exhibits an equatorial CT centered along ~ 1° S and a strong frontal zone extending from the equator to ~ 5° S, with SST at its center decreasing monotonically eastward and then connecting to the coastal upwelling zone south of the equator (Deser & Wallace, 1990). The CT and the frontal zone are nearly always present but their strength varies both seasonally and on an interannual time scale. The cross-equatorial southerlies are the major mechanism for sustaining the CT east of 90° W by inducing upwelling slightly south of the equator. The equatorial zonal

asymmetry is primarily sustained by interaction of the CT and easterly winds (Dijkstra and Neelin 1995), which also plays an important role on the development of El Niño - Southern Oscillation (ENSO) (Wang and Picaut 2004). The SST meridional asymmetry plays an important role in the northward displacement of the ITCZ, with zonal band of warm water with SST greater than 27° C around 10° N that supports deep convection and much colder water on the south side of the equator with significantly weaker precipitations. The north–south asymmetry is sustained robustly by the surface heat flux and ocean mixed-layer temperature interactions (Xie and Philander 1994; Philander et al. 1996).

The seasonal cycle in the SEP follows the Southern Hemisphere, but is delayed by a month or two. The “cold season” extends from July to November, and the “warm season” from February to April. The southerly wind flow is almost twice as strong during the cold season during which the CT is more prominent and the ITCZ is located farther north. The ITCZ reaches its southernmost position in March and then moves northward until September in response to the increase in solar radiation and SST in the Northern Hemisphere. During a brief period from March to April, the eastern tropical Pacific climate becomes rather symmetrical, with an ITCZ forming over a warm SST band on either side of the equator (Xie and Philander 1994), indicating a strong SST control, which is most effective in the eastern Pacific apparently because high SSTs are restrained in narrow zonal bands surrounded by high gradients (Xie et al. 2007). The meridional SST gradient between the equator and ITCZ varies by about a factor of three between the warm and cold years. The sea level pressure has a stronger meridional gradient during the cold season than during the warm season. Cloudiness is high during the cold season and low during the warm season, between the equator and 20°S, excluding a narrow latitudinal band that emerges with the briefly seasonal southern

incursion of the ITCZ. As the northern ITCZ and cross-SST frontal advection weakens in March, the cloud band north of the equator debilitates. Alternatively during the boreal summer and fall, part of this cloud band increases when both the ITCZ and the southerly cross-frontal flow intensifies. In general, the eastern Pacific (including the equator) is cloudier in September than March, contributing to the annual cycle in equatorial SST (Yu and Mechoso 1999).

During the warm years the stronger meridional pressure gradient are observed to the south of the CT, whereas during the cold years they are observed to the north of the CT. In addition, on warmer years the strength of the southerly winds increases from the Southern Hemisphere Tropics to a maximum approximately located at 3° - 4° N, whereas during the colder years the southerly winds decelerate as they approach the CT and then accelerate sharply as they cross the oceanic frontal zone (~5° N) (Wallace et al. 1987).

The prevailing easterly trade winds, the southeast– northwest tilt of the coastal line of the tropical Pacific favors coastal upwelling south of the equator (Philander et al. 1996). The coastal SST asymmetry generates coupled waves due to positive ocean–atmosphere feedback that propagates climatic asymmetry westward across the Pacific basin (Xie 1996; Ma et al. 1996). The wind–evaporation–SST (WES) feedback is at work to sustain latitudinal asymmetry over the Pacific (Xie and Philander 1994). In September, when SSTs are at their highest in the Northern Hemisphere and a lowest in the Southern Hemisphere, the Equatorial winds intensify and then weaken in March when the seasonal cycle in off-equatorial SST reverses sign. In connection with the seasonal migration of the ITCZ, the largest wind differences between March and September are located north of the equator. On the other hand, the largest SST differences are located on and south of the equator due to a shoaling of the thermocline that produces SST

sensitive to wind changes. The equatorial SSTs cools in September, as direct response of an intensification of the southeast trades, which strengths the upwelling, vertical mixing, and surface evaporation (Mitchell and Wallace 1992; Xie 1994).

Garreaud and Battisti (1999) and Zhang et al. (1997) established that the subtropical South Pacific is dominated by anomalies out of phase with the ones occurring in the tropical Pacific, centered about 30° S.

The South Pacific's subtropical gyre dictates the horizontal circulation in the South Pacific Ocean. The ocean's circulation is composed of four major currents (Tomczak and Godfrey, 1994):

- The South Equatorial Current (SEC), with westward flow just a few degrees south of the equator.
- The East Australian current, a western boundary current with poleward flow.
- The East Australian current.
- The eastward South Pacific Current (SPC), with a flow along the Subtropical Front, concentrated at 40˚S in the western Pacific and at 30° – 35° S in the eastern Pacific.
- The Humboldt Current (HC), an eastern boundary current with equatorward flow also known as the Peru Current.

Tsimplis et al. (1998) calculated the transport of upper 700 m between the East Pacific Rise (120˚W) and the South America coast to 18 Sverdrups (Sv) across 32.5˚S and 14 Sv across 17˚S.

The HC initiates approximately around 35° and 40° S, on 800 km wide band offshore of southern Chile; with maximum geostrophic velocities not surpassing 10 cm s^{-1}. It expands and increases in width, to about 15° S to continue northward, offshore and parallel to the Peruvian coast, connecting with the equatorial currents (Strub et al., 1998 and Tomczak and Godfrey, 1994). The current flows close to the

coast, on the inner 500 km offshore of the southern Chile, but not following the coastline, and it shifts further offshore in northern Chile, nourishing the SEC to some extent. The SEC is more intense, originating west of 90° W, and located in the region between 5° and 15° S. It primarily has a westward stream, with an intensify core around 5° and 10° S, with geostrophic velocities moderately greater than 20 cm s^{-1} west of 100° W (for a detail explanation of the SPC general circulation, see Strub et al., 1998, Tomczak and Godfrey, 1994 and Fuenzalida et al., 2008).

An important feature of the HC is a 250 km wide, jet-like core with velocities above 15 cm s^{-1}, originating less than 200 km off southern Chile at approximately at 40° S / 75° W in summer and in winter 38° S / 76° W. The current streams northward, augmenting its distance from the Chilean coast by shifting a few degrees to the west, with an significant bifurcation at 23° S / 79° W, generating a coastal ramification bearing in the direction of the southern Peruvian coast around 15° S, and an oceanic ramification with a seasonal flow direction; north-northwesterly in winter and northwesterly in summer. A year-round retention zone is persistent between both ramifications year-round, although it is more pronounced in summer. The HC is narrower to some extent from its southern origin to the ramification point, strengthening by 2 to 3 cm s^{-1} in summer in contrast to the winter (Shaffer & al. 2004, Chaigneau and Pizarro 2005, Fuenzalida et al. 2008). On the contrary, coastal ramification off the Peruvian coast intensifies by 2 to 3 cm s^{-1} and becomes wider in winter (Pauly & Tsukayama 1987, & Fuenzalida et al. 2008).

The SPA's seasonal meridional movement cycle governs the wind stress patterns in the SEP, and consequently forces the subtropical gyre and the HC's seasonal differences in width, location and intensity. The SPA has a southern location in summer centered on 35° S / 90° - 100° W and more north during the winter centered on

30° S / 90° - 100° W (Bakun and Nelson, 1991). On the Pacific South American coast, the wind stress runs along-shore towards the equator, starting on the south Chilean coast (35° S / 40° S), to then turning to the northwest around 25° S / 80° W (off shore form the northern Chilean coast) and following the southeast–northwest tilt of the Peruvian coastline (from the coast up to 120° W approximately). The south Chilean coast's along-shore wind stress is nourished by the southern branch on the SPA with eastward or east-southeastward flow. The strongest wind stress areas during summer and winter are located within the westerlies and the coastal upwelling areas in Peru and northern Chile. With the exception of the nucleus of the HC (off central-southern Chile), the wind stress in the SEP (5°- 45° S / 150° - 75° W) is weaker in the summer and strongest in winter (Fuenzalida et al. 2008).

In general wind stress curl is closely related to meridional Sverdrup transport; in the Southern Hemisphere, positive values result in an equatorward flow and downwelling, and negative values result in a poleward flow and upwelling. The majority of the SEP has anticyclonic (positive) wind stress curl, mostly offshore, and cyclonic (negative) curl near the continental boundaries, restricted by the 5° S latitude, the Peruvian coast, and an area linking southern Peru with the zone at 5° S around 135° / 145° W, and a smaller region off northern Chile. In summer, wind stress curl is stronger off the coast of Chile, with an HC's acceleration core offshore of central-southern Chile south of 35° S, generated by a center of strong wind stress curl. During the winter, the wind stress curl strengthened center moves northward about 8° latitude with a zonal strip of higher wind stress curl producing a shift offshore of the HC to central-northern Chile. Also, during winter the positive wind stress curl considerably extends equatorward, therefore generating a northward shift of the subtropical gyre (Fuenzalida et al. 2008).

ENSO can be understood as an irregular low frequency interannual climate oscillation between abnormally warm stages (EN) and cold stages (La Niña), with global influence, projecting beyond the tropical Pacific through atmospheric teleconnections that affect patterns of weather variability worldwide. These two phases of the tropical Pacific materialize from a background of “normal” state, which displays a large amount of meteorological and oceanographic noise. EN typically occurs at intervals of 2 - 7 years (strong events every 13 - 70 years: e.g. 1925 - 1926, 1982 - 1983 and 1997 - 1998) with an average return period of 4 years (Quinn et al 1987, McPhaden 2006). EN and La Niña (LN) develop in association with swings in the Southern Oscillation, lasting between half a year to several years in duration (McPhaden 1999). Therewith, ENSO constitutes the major intra-decadal variability in the Humboldt Current Ecosystem (HCE).

Currently it is well known that the SST positive anomalies in the eastern Pacific during EN events are predominantly remotely forced (Cronin and Kessler 2002, McPhaden 2006), on the basis that coastal winds over the eastern Pacific are usually upwelling-favorable and only change late in the event, if at all, and therefore not able to produce the observed eastern coastal warming (McPhaden 1999, Carr et al., 2002). Wind-forced variability in the western Pacific produces dramatic changes in thermocline depth and currents which are transmitted eastward by equatorial Kelvin waves (McPhaden, McPhaden 1995, Cronin and Kessler 2002). The equatorial thermocline is flattened across the Pacific due to westerly anomalies on the western and central basin, which also reduces the SEC flow (McPhaden 1999, Wang and McPhaden 2000, Yu and Hsie 2006). All along the equator, the eastward current anomalies propagate, therefore warming the western and central Pacific, primarily by advection, however it is most likely that the warm west Pacific water mass is not transported all the way to the Peruvian coast (Kessler and McPhaden, 1995, Picaut et al. 1996). The warming on the east is

fundamentally driven a change in local surface fluxes, heating the surface layer, as a consequence of a deeper thermocline. The easterly winds continue to blow under near to normal conditions; however only warm water is upwelled due to a deeper thermocline. The warmer water that now reaches the surface produce a positive feedback, since warmer SST predisposes a restrain on the development of the normal stratus decks in the eastern Pacific, thus permitting additional local warming (Kessler and McPhaden, 1995, Cronin and Kessler, 2002) In general, during EN, the highest SST and eastward zonal current anomalies reach their highest values in September of the year with the largest wind anomalies, however the warmest SSTs develop in January–March of the following year, indicating that EN events are phase-locked with the annual cycle. Consequently, EN emerges in the east as a suppression of the cold phase of the annual cycle (Wang and Fiedler, 2006).

The ENSO related SST anomalies exhibit largest magnitudes along the equator, decreasing over a wide, wedge-shaped region that spreads poleward along the eastern boundaries (Enfield & Mestas-Nuñez, 1999). ENSO-related SST variability decreases poleward from subtropical latitudes, while interdecadal variability increases from subtropics to midlatitudes. Montecinos et al. (2003) demonstrated that along the coast of western South America the standard deviation of detrended SST anomalies decrease almost linearly with latitudes from the equator to 23 °S (16 °S), then becoming constant to the south (see their Figure 2).

B. DESCRIPTION OF THE PARALLEL CLIMATE MODEL

B.1. The Parallel Climate Model

The United States Department of Energy (DOE) sponsored a pilot project, under the Accelerated Climate Prediction Initiative, to accelerate and extend the modeling state and to reduce the existing uncertainties about long-term climate change, and at the same time provide regional information in climate change projections to support national and international energy and environmental policies that must be formulated and implemented early next decade (ACPI 1998).

The ACPI project was funded to initialize Coupled General Circulations Models (CGCMs) with observed conditions for current climates. These CGCMs subject to the ACPI initialization use the BAUS of emissions as well as the radiative forcings, and its results are used to develop the dynamic downscaling for regional climate change assessment, to improve the representation of the topography influence on local climate and to give climate information at the scales required for simulating hydrological response (Dai et al. 2003; Barnett et al. 2003).

The Parallel Climate Model version 1 is a CGCM used by the ACPI to simulate global climate response under the BAUS during the 21st century (2000-2100). The coupled climate system model PCM is composed of an atmospheric general circulation model, an ocean global model, a land model, and a sea-ice model, coupled through a flux coupler element that performs the computing of the interfacial fluxes among the component models. Because the horizontal grids differences between the component models, an interpolation scheme is utilized to perform an area-preserving mapping of the data. The flux coupler also scales fluxes as necessary to conserve the total global energy exchange between the components (Washington et al. 2000).

These components from the global circulation models are the atmospheric GCM Community Climate Model version 3 (CCM3) with T42 resolution (~2.9 degree), Los Alamos National Laboratory Parallel Ocean Program (POP) which has an average

resolution of 2/3° latitude and longitude, with an enhanced latitudinal resolution of 0.5 degrees near the Equator, a land biophysics model which has a T42 resolution, and a dynamic-thermodynamic sea-ice model with 27 km x 27 km (0.25 degree) of resolution over the Arctic Ocean (Dai et. al. 2003).

For supplemental information on the characteristics of the PCM used on r the IPCC AR4, please visit the Program for Climate Model Diagnosis and Intercomparison (PCMDI) model information web page at: http://www-pcmdi.llnl.gov/ipcc/model_documentation/PCM.htm

B.2. Atmospheric/Land Component

The atmospheric component of PCM performs the simulation of the synoptic interactions among several atmospheric fields, either vectorial or scalar. CCM3 includes latest versions of radiation, boundary physics and precipitation physics. In addition, it considers the Land-Surface Model (LSM) which takes into account the soil physics and vegetation (Washington et al. 2000).

The CCM developed by NCAR Climate and the Global Dynamics (CGD) Division provides a three-dimensional global model. CCM has made significant improvements since early CCM0A, especially with the CCM version 2 (CCM2) such as clouds and radiation, moist convection, the planetary boundary layer, and diurnal cycle among others. CCM2 also employ a T42 spectral resolution (~ 2.9 x 2.9 degree transform grid), a terrain-following hybrid 18 vertical coordinate and a rigid lid at 2.917 mb (Kiel et al. 1998).

The fourth generation of the CCMs is the CCM version 3 (CCM3). CCM3 is a spectral model with T42 resolution and 18 vertical levels (Kiel et al. 1998) and it is more suitable to carry out the coupling of land, ocean and sea-ice component models.

Changes in the long wave parameterization were made, incorporating the trace gases CH4, N2O, CFC11, CFC12, together with CO2, O3, H2O gases, and also incorporating the 0.14 aerosol optical depth. The aerosol optical depth has been adjusted experimentally to get a globally and annually averaged balance between incoming and outgoing radiation.

The longwave parameterization is used to compute the radiative flux at each model layer for , , , as a function of their band absorbance, path length, transmission, layer extinction optical depth, etc. After the fluxes are calculated a model energy balance is carried out for each layer (William et al 2004). In addition, the needed input data about the greenhouse gasses are ingested by means of netcdf standard files (time-variant boundary dataset for tracer emissions). The CO2 is ingested homogenously distributed over the globe. Improvements of the cloud optical properties consisted of diagnosing the effective radius and liquid water path, and incorporating radiative properties of ice clouds. A LSM1 is included in CCM3 running both models at the same grid resolutions. LSM1 is a one-dimensional model of momentum, energy, water and exchange between the atmosphere and land. This LSM1 model is able to differentiate the vegetation types, bare soil and different soil type, lakes and wetlands and is treated separately within each grid cell (Boville and Hurrel 1998). The ocean surface roughness is computed as a function of the surface wind speed, resulting in more realistic surface flux. The parameterized convection was modified resulting in a reduction of the hydrologic cycle magnitude and a smoother distribution of the tropical distribution.

B.3. Ocean Component

The PCM ocean component uses the POP developed by the LANL sponsored by the Department of Energy's The Climate Change Program (CHAMMP) program. CHAMMP has the most important component links to the emerging technologies in High Performance Computing with improved numerical accuracy and computationally efficient climate models (LANL 2003).

The ocean circulation model, POP, solves the three-dimensional primitive equations for fluid motions in spherical polar-vertical z coordinates, under Boussinesq and hydrostatic approximations, to describe the ocean dynamics. These equations are the momentum equations, continuity equations, tracer equations, equations of states and hydrostatic equation, where the prognostic necessary variables to predict the oceanic behavior are; eastward and northward velocity, the vertical velocity, the pressure, the water density, the potential temperature and salinity. The tracer transport equation considers the total freshwater flux per unit area as a consequence of the balance among the precipitation, evaporation, river runoff, freezing and melting of sea ice; the change in volume of the surface layer due to undulations of the free surface is also considered into the tracer transport equation. An anisotropic medium in respect to viscosity and a no-slip boundary condition are also considered. POP ocean circulation model solves the baroclinic tendencies using the leapfrog scheme, while the barotropic modes are integrated through an implicit free surface formulation to solve the two-dimensional surface pressure (LANL 2003).

A standard latitude-longitude grid is mapped onto a sphere generating singularities at the Poles, while the use of the orthogonal horizontal grid makes possible to move the singularities into an adjacent landmass; these dipole grids, in the Northern Hemisphere, can place the singularity over North America, Greenland or Asia (see

Figure This approach used by POP permits a singularity-free grid in the Arctic Ocean, but also the mesh is made to have a smooth transition from the northern Equator to southern hemisphere polar grid that usually is a Mercator grid. An interactive procedure is used to construct the semianalytic dipole grid and in this manner the equator continues being a grid line, while the Southern Hemisphere has a pole in the true South Pole (LANL 2003). There is special treatment given to various straits and bottom topography to obtain near observed ocean flow transport.

B.4. Sea Ice Component

The sea-ice component is a fully dynamic-thermodynamic model, adapted by the Naval Postgraduate School (see Zhang and Hibler, 1997 for major references) and optimized for massively parallel processor (MPP) architecture by A. Craig of NCAR. The grid is transformed such that the resolution is constant, thus avoiding the problem of convergence near the pole as on a latitude-longitude grid. This grid will require an additional interpolation of atmosphere and ocean variables. The spatial resolution of Zhang's model is about 18 km, which provides a realistic Arctic simulation of eddy resolving ocean and sea ice motion.

The model predicts the evolution of ice thickness, ice concentration, velocity, snow thickness, and surface temperature of the ice (and snow-covered sea ice) in response to winds, ocean currents, air and ocean temperatures, humidity, radiation an internal stresses. The sea-ice model also computes leads.

The ice model grid is transformed such that the resolution is constant, thus avoiding the problem of convergence near the pole as on a latitude-longitude grid. This

grid will require an additional interpolation of atmosphere and ocean variables. The spatial resolution of the model is 27 km, and the grid is centered over each pole.

B.5. Model Initialization

The radiative fluxes through atmospheric and the interfacial fluxes of heat, mass and momentum, are exchanged among the components models, must be in balance at the beginning of a simulation. The initialization of the couple system was done by integrating the atmosphere daily for 10 years with specified SSTs and observed sea-ice concentrations; this allows the soil temperature and moisture to come into quasi–equilibrium with the atmosphere. The last five years of the atmospheric output were used for forcing the ocean and sea-ice system, and then the ocean was run with restoring to observed values of temperature and salinity. The ocean/ice system is spin-up for 86 years with repeated five years of atmospheric years. The deeper ocean temperature and salinity were accelerated towards equilibrium, although they were not in equilibrium at the end of this spin-up due to the immense thermal and the time scale to change overall salinity by surface flux changes (Washington et al. 2000).

It must take into account, that the model has different sources of error on the atmospheric fluxes, especially in the cloud formulation and assignment of radiative forcing and boundary layer exchanges, heat, moisture and momentum.

The initialization provided an initial climate state compatible with the observed SST distribution, preserving it in long-term simulations without any change in radiative forcing. Then, the coupled model is run for 50 years as an adjustment period where changes to the aerosol background was made (from 0.14 to 0.08) to force the global net surface imbalance from about -1 Wm^{-2} to near zero at the end of this period.

Subsequently, the coupled system was run for 300 years to establish the control experiment, used as initial condition for different forcing experiments. The control experiment has no anthropogenic, solar variability, or volcanic forcing.

B.6. PCM General Features

Washington et al. (2000) performed forcing experiments of : 0.5% per year increase to the time of doubling, and 1 % per year increase with idealized stabilization at doubling and quadrupling . The transient experiment (1 % increase per year) had a starting concentration of 355 PPM achieving doubling (710 PPM) near year 70, with an average warming of 1.27° C (10 year mean from years 66 to 75) and a warming of 2.89° C (10 year mean from years 66 to 75). The 0.5% has a warming of 1.49° C (mean of years 136-145) at the doubling point. Global averaged sea level rise is nearly 7 cm at the time of doubling and 23 cm at the time of quadrupling. After the doubling point and stabilization, the surface temperature has a small continuous warming. After the quadrupling point and stabilization the warming rate is larger for more than 50 years. Changes of the ocean temperature are depth dependant, with variations ranging to several tenths of degree Celsius (mostly in the upper ocean) to lesser amount in the deeper parts.

C. PCM RUNS DESCRIPTION

C.1. Control Runs

B06.18. 1870 fully coupled equilibrium run date

Integration years: 0140-09 to 0389-02

Years Used: 0141-0190,0210-0259, 0320-0369

More details:

https://www.earthsystemgrid.org/metadata/showObject.do?id=ucar.cgd.pcm.B06.18&schema=esg

B06.62. 1870 fully coupled equilibrium run date

Integration years: 0450-11 to 1204-04

Years Used: 0460-509, 0550-0599

More details:

https://www.earthsystemgrid.org/metadata/showObject.do?id=ucar.cgd.pcm.B06.62&schema=esg

C.2. Historical Runs

B06.08. Historical 1870-1999 GHG, Sulfate, Ozone forcing

Integration years: 1870-09 to 1999-12

Control Initialization: .02, 0140-0901

Years Used: 1950-1999

More details:

https://www.earthsystemgrid.org/metadata/showObject.do?id=ucar.cgd.pcm.B06.08&schema=esg

B06.22. Historical 1870-1999 GHG, Sulfate, Ozone forcing

Integration years: 1870-03 to 1999-12

Control Initialization: .18, 0160-0301

Years Used: 1950-1999

More details:

https://www.earthsystemgrid.org/metadata/showObject.do?id=ucar.cgd.pcm.B06.22&schema=esg

B06.23. Historical 1870-1999 GHG, Sulfate, Ozone forcing

Integration years: 1870-03 to 1999-12

Control Initialization: .18, 0150-0301

Years Used: 1950-1999

More details:

https://www.earthsystemgrid.org/metadata/showObject.do?id=ucar.cgd.pcm.B06.23&schema=esg

C.3. IPCC Runs

B06.20. IPCC A2 Scenario

Integration years: 1980-03 to 2099-12

Initialization: as branch from B06.08, year 1980-0301.

Years Used: 2000-2049, 2050-2099

More details:

https://www.earthsystemgrid.org/metadata/showObject.do?id=ucar.cgd.pcm.B06.20&schema=esg

B06.21. IPCC B2 Scenario

Integration years: 2000-12 to 2099-12

Control Initialization: as branch from B06.20, year 1999-1201.

Years Used: 2001-2050, 2050-2099

More details:

https://www.earthsystemgrid.org/metadata/showObject.do?id=ucar.cgd.pcm.B06.22&schema=esg

REFERENCES

Agenbag, J. J., et al. "Estimating environmental preferences of South African pelagic fish species using catch size and remote sensing data." Progress in Oceanography 59.2-3 (2003): 275-300.

Alheit, J., and M. Niquen. "Regime shifts in the Humboldt Current Ecosystem." Progress in Oceanography 60.2-4 (2004): 201-222.

An, S. I., and F. F. Jin. "An Eigen analysis of the interdecadal changes in the structure and frequency of ENSO mode." Geophysical Research Letters 27.16 (2000): 2573-2576.

An, S. I., and B. Wang. "Interdecadal change of the structure of the ENSO mode and its impact on the ENSO frequency." Journal of Climate 13.12 (2000): 2044-2055.

Arblaster, J. M., G. A. Meehl, and A. M. Moore. "Interdecadal modulation of Australian rainfall." Climate Dynamics 18.6 (2002): 519-531.

Arntz, W. E. and Fahrbach, E. El Niño. Experimento climático de la naturaleza, causas físicas y efectos biológicos. México City, México Fondo de Cultura Económica, México, 1996.

Arntz W. E., Gallardo V.A., Gutiérrez D., Isla E., Levin L.A., Mendo J., Neira C., Rowe G.T., Tarazona J., Wolff M. "El Niño and similar perturbation effects on the benthos of the Humboldt, California, and Benguela current upwelling ecosystems." Ad Geo 6 (2006): 243-265.

Ayon, P., S. Purca, and R. Guevara-Carrasco. "Zooplankton volume trends off Peru between 1964 and 2001." Ices Journal of Marine Science 61.4 (2004): 478-484.

Bakun, A. "Global climate change and intensification of coastal ocean upwelling." Science 247.4939 (1990): 198-201.

Bakun, A. Patterns in the ocean: Ocean processes and marine population dynamics.: University of California Sea Grant, San Diego, California, USA, in cooperation with Centro de Investigaciones Biologicas de Noroeste, La Paz, Baja California Sur, Mexico., 1996.

Bakun, A., and K. Broad. "Environmental 'loopholes' and fish population dynamics: Comparative pattern recognition with focus on El Niño effects in the Pacific." Fisheries Oceanography 12.4-5 (2003): 458-473.

Bakun, A., and C. S. Nelson. "The seasonal cycle of wind-stress curl in subtropical eastern boundary current regions." Journal of Physical Oceanography 21.12 (1991): 1815-1834.

Barber, R. T., and F. P. Chavez. "Biological consequences of El Niño." Science 222.4629 (1983): 1203-1210.

Barber, R. T., and R. L. Smith. Coastal upwelling ecosystems. Analysis of marine ecosystems. Ed. A. R. Longhurst: Academic Press, London, New York etc., 1981.

Barnett, T., R. Malone, W. Pennell, D. Stammer, A. Semtner, and W. Washington. "The effects of climate change on water resources in the west: Introduction and overview." Climatic Change 62 (2004): 1-13.

Bertrand, A., et al. "From small-scale habitat loopholes to decadal cycles: A habitat-based hypothesis explaining fluctuation in pelagic fish populations off Peru." Fish and Fisheries 5.4 (2004): 296-316.

Bjerknes, J. "Large-scale atmospheric response to the 1964-65 pacific equatorial warming." Journal of Physical Oceanography 2.3 (1972): 212–217.

Boer, G. J., et al. "Is there observational support for an el Niño-like pattern of future global warming?" Geophysical Research Letters 31.6 (2004): 4.

Bouchon, M., Cahuin, S., Diaz, E. and Niquen, M. "Captura y esfuerzo pesquero de la pesquería de anchoveta peruana (Engraulis ringens)." Boletín del Instituto del Mar del Perú 19 (2000): 109–115.

Boville, B. A., and J. W. Hurrell. "A comparison of the atmospheric circulations simulated by the CCM3 and csm1." Journal of Climate 11.6 (1998): 1327-1341.

Brochier, T., et al. "An individual-based model study of anchovy early life history in the northern Humboldt current system." Progress in Oceanography 79.2-4 (2008): 313-325.

Buse, H. Actividad pesquera. Ed. Documenta. Lima, Peru: Editorial Andina S.A., 1981.

Cane, M. A. "The evolution of el Niño, past and future." Earth and Planetary Science Letters 230.3-4 (2005): 227-240.

Carr, M. E. "Estimation of potential productivity in eastern boundary currents using remote sensing." Deep-Sea Research Part Ii-Topical Studies in Oceanography 49.1-3 (2002): 59-80.

Carr, M. E., and K. Broad. "Satellites, society, and the Peruvian fisheries during the 1997-98 el Niño " Satellites, oceanography and society. Ed. D. Halpern. New York Elsevier Science, 2000. 171-191.

Carranza, L. "Contracorriente marina observada en Paita y Pacasmayo." Bol. de la Soc. Geogr. de Lima 1 (1891): 344-345.

Carrillo, C. "Hidrografía oceánica." Bol. de la Soc. Geogr. de Lima 2 (1892): 72-110.

Castillo, J., Barbieri, M. A., & Gonzalez, A. "Relationships between sea surface temperature, salinity, and pelagic fish distribution off northern Chile." ICES Journal of Marine Science 53.2 (1996): 139–146.

Castro, L. R., and E. H. Hernandez. "Early life survival of the anchoveta Engraulis ringens off central Chile during the 1995 and 1996 winter spawning seasons." Transactions of the American Fisheries Society 129.5 (2000): 1107-1117.

Chaigneau, A., and O. Pizarro. "Mean surface circulation and mesoscale turbulent flow characteristics in the eastern south pacific from satellite tracked drifters." Journal of Geophysical Research-Oceans 110.C5 (2005): 17.

Chavez, F. P., et al. "From anchovies to sardines and back: Multidecadal change in the Pacific Ocean." Science 299.5604 (2003): 217-221.

Clarke, A. J., and A. Lebedev. "Remotely driven decadal and longer changes in the coastal Pacific waters of the Americas." Journal of Physical Oceanography 29.4 (1999): 828-835.

Cohen, J., Cohen P., West, S. G., & Aiken, L. S. Applied multiple regression/correlation analysis for the behavioral sciences. 3rd ed. Hillsdale, NJ: Lawrence Erlbaum Associates, 2003.

Collins, M. "El Niño- or La Niña-like climate change?" Climate Dynamics 24.1 (2005): 89-104.

Cronin, M. F., and W. S. Kessler. "Seasonal and interannual modulation of mixed layer variability at 0 degrees, 110 degrees W." Deep-Sea Research Part I-Oceanographic Research Papers 49.1 (2002): 1-17.

Csirke, Jorge, et al. "[status of resources of anchovy (Engraulis ringens) and sardine (Sardinops sagax) at the beginning of 1994 and perspectives for fishing in Peru, with particular reference to the northern and central regions of the Peruvian coast.]." Boletin Instituto del Mar del Peru (Callao) 15.1 (1996): 1-23.

Cury, P., et al. "Small pelagics in upwelling systems: Patterns of interaction and structural changes in "Wasp-waist" Ecosystems." ICES/SCOR Symposium on Ecosystem Effects of Fishing. (1999): 603-618.

Dai A., Washington W.M., Meehl G. A., Bettge T. W., and Strand W. G. "The ACPI climate change simulations." Climate Change for the ACPI Special Issue. 1(2003): 1-23 pp.

Deser, Clara, and John M. Wallace. "Large-scale atmospheric circulation features of warm and cold episodes in the tropical pacific." Journal of Climate 3.11 (1990): 1254-1281.

Dijkstra, H. A., and J. D. Neelin. "Ocean-atmosphere interaction and the tropical climatology. II: why the Pacific cold tongue is in the east." Journal of Climate 8.5 (1995): 1343-1359.

Eguiguren, D.V. "Las lluvias de Piura." Bol. de la Soc. Geogr. de Lima 4 (1894): 241-258.

Emery, W. J., and R. E. Thomson. Data analysis methods in physical oceanography. 2nd. ed. Amsterdam, The Netherlands: Elsevier, 2004.

Enfield, D. B., and A. M. Mestas-Nunez. "Multiscale variabilities in global sea surface temperatures and their relationships with tropospheric climate patterns." Journal of Climate 12.9 (1999): 2719-2733.

Escribano, R., et al. "Biological and chemical consequences of the 1997-1998 El Niño in the Chilean coastal upwelling system: A synthesis." Deep-Sea Research Part Ii-Topical Studies in Oceanography 51.20-21 (2004): 2389-2411.

Espino, M. "'variability is normality'." Ed. G. Passalacqua. Lima1999.

Fedorov, A. V., and S. G. Philander. "Is el Niño changing?" Science 288.5473 (2000): 1997-2002.

Fiedler, P.C. "Environmental change in the eastern tropical pacific ocean: Review of ENSO and decadal variability." Marine Ecology Progress Series 244 (2002): 265–283.

Field, D. B., et al. "Planktonic foraminifera of the California current reflect 20th-century warming." Science 311.5757 (2006): 63-66.

Fuenzalida, R., et al. "Satellite altimetry data reveal jet-like dynamics of the Humboldt current." Journal of Geophysical Research-Oceans 113.C7 (2008): 11.

Garreaud, R. D., and D. S. Battisti. "Interannual (ENSO) and interdecadal (ENSO-like) variability in the southern hemisphere tropospheric circulation." Journal of Climate 12.7 (1999): 2113-2123.

Glantz, M. H. "Floods, fires, and famine - is el-Niño to blame." Oceanus 27.2 (1984): 14-19.

Guilyardi, E., et al. "Representing el Niño in coupled ocean-atmosphere GCMs: The dominant role of the atmospheric component." Journal of Climate 17.24 (2004): 4623-4629.

Gutierrez, M. "Efectos del evento el Niño 1997–98 sobre la distribución y abundancia de anchoveta (Engraulis ringens)." El Niño en América Latina: Impactos biológicos y sociales. Ed. W.E. Arntz and E. Castillo de Maruenda J. Tarazona. Lima, Perú: Consejo Nacional de Ciencia y Tecnología, 2001. 55–72.

Gutierrez, M., et al. "Anchovy (Engraulis ringens) and sardine (Sardinops sagax) spatial dynamics and aggregation patterns in the Humboldt Current ecosystem, Peru, from 1983-2003." Fisheries Oceanography 16.2 (2007): 155-168.

Hoerling, M. P., and A. Kumar. "Atmospheric response patterns associated with tropical forcing." Journal of Climate 15.16 (2002): 2184-2203.

IPCC, ed. Climate change 2007 - the physical science basis: Contribution of working group I to the fourth assessment report of the Intergovernmental Panel on Climate Change [Solomon, s., d. Qin, m. Manning, Z. Chen, M. Marquis, K.B. Averyt, M.Tignor and H.L. Miller (eds.)]. Cambridge: Cambridge University Press, 2007.

Joseph, R., and S. Nigam. "ENSO evolution and teleconnections in IPCC's twentieth-century climate simulations: Realistic representation?" Journal of Climate 19.17 (2006): 4360-4377.

Kearns, E. J., and M. E. Carr. "Seasonal climatologies of nutrients and hydrographic properties on quasi-neutral surfaces for four coastal upwelling systems." Deep-Sea Research Part Ii-Topical Studies in Oceanography 50.22-26 (2003): 3171-3197.

Kessler, W. S., and M. J. McPhaden. "The 1991-1993 El Niño in the central pacific." Deep-Sea Research Part Ii-Topical Studies in Oceanography 42.2-3 (1995): 295-333.

Kiehl, J. T., et al. "The National Center for Atmospheric Research Community Climate Model: CCM3." Journal of Climate 11.6 (1998): 1131-1149.

LANL. "Parallel Ocean Program (POP)." User Guides: Los Alamos National Laboratory, 2003. 1-75. Vol. 1.

Laurs, R. M., Fiedler, P. C., & Montgomery, D. R. "Albacore tuna catch distributions relative to environmental features observed from satellites." Deep-Sea Research 31 (1984): 1085–1099.

Lluch-Belda, D., et al. "Worldwide fluctuations of sardine and anchovy stocks - the regime problem." South African Journal of Marine Science-Suid-Afrikaanse Tydskrif Vir Seewetenskap 8 (1989): 195-205.

Lluch-Belda, D., et al. "Sardine population expansion in eastern boundary systems of the pacific ocean as related to sea surface temperature." South African Journal of Marine Science (1992): 147-155.

Ma, C. C., et al. "Peruvian stratus clouds and the Tropical Pacific circulation: A coupled ocean-atmosphere GCM study." Journal of Climate 9.7 (1996): 1635-1645.

Mantua, N. J., and S. R. Hare. "The Pacific Decadal Oscillation." Journal of Oceanography 58.1 (2002): 35-44.

Maravelias, C. D., and D. G. Reid. "Relationship between herring (Clupea harengus, L) distribution and sea-surface salinity and temperature in the northern north-sea." Scientia Marina 59.3-4 (1995): 427-438.

Margalef, R. and Estrada, M. "On upwelling, eutrophic lakes, the primitive biosphere, and biological membranes." Coastal upwelling. Ed. F.A. Richards. Washington, D.C.: American Geophysical Union, 1981. 522-529.

McFarlane, G. A., et al. "Climate variability and pacific sardine populations and fisheries." Fisheries in a changing climate. Ed. Nature A. McGinn. American Fisheries Society Symposium: Volume 32: American Fisheries Society, 2002. 195-214.

McGregor, H. V., et al. "Rapid 20th-century increase in coastal upwelling off northwest Africa." Science 315.5812 (2007): 637-639.

McPhaden, M. J. "The tropical atmosphere ocean array is completed." Bulletin of the American Meteorological Society 76.5 (1995): 739-741.

McPhaden, M. J., and X. Yu. "Equatorial waves and the 1997-98 El Niño." Geophysical Research Letters 26.19 (1999): 2961-2964.

McPhaden, M. J., S. E. Zebiak, and M. H. Glantz. "ENSO as an integrating concept in earth science." Science 314.5806 (2006): 1740-1745.

Meehl, G. A., et al. "Factors that affect the amplitude of El Niño in global coupled climate models." Climate Dynamics 17.7 (2001): 515-526.

Meehl, G. A., and H. Y. Teng. "Multi-model changes in el Niño teleconnections over North America in a future warmer climate." Climate Dynamics 29.7-8 (2007): 779-790.

Meehl, G. A., H. Y. Teng, and G. Branstator. "Future changes of el Niño in two global coupled climate models." Climate Dynamics 26.6 (2006): 549-566.

Meehl, G. A., et al. "Factors affecting climate sensitivity in global coupled models." Journal of Climate 17.7 (2004): 1584-1596.

Mitchell, T. P. and J. M. Wallace. "On the annual cycle in equatorial convection and sea surface temperature." Journal of Climate 5 (1992): 1140-1156.

Montecinos, A., S. Purca, and O. Pizarro. "Interannual-to-interdecadal sea surface temperature variability along the western coast of South America." Geophysical Research Letters 30.11 (2003): 4.

Niquen, C. M., Bouchon, C. M., Cahuín, V. S., and Díaz, A. E. "Pesquería de anchoveta en el Mar Peruano." Boletín Instituto del Mar del Perú 19 (2000): 109-115.

Niquen, M., and M. Bouchon. "Impact of el Niño events on pelagic fisheries in Peruvian waters." Deep-Sea Research Part II - Topical Studies in Oceanography 51.6-9 (2004): 563-574.

Orlove, B. S., K. Broad, and A. M. Petty. "Factors that influence the use of climate forecasts - evidence from the 1997/98 el Niño event in Peru." Bulletin of the American Meteorological Society 85.11 (2004): 1735-+.

Patrinos, A. "Bringing the promise of simulation to the challenge of climate change." June 1998 ed: The Accelerated Climate Prediction Initiative, 1998. http://www.csm.ornl.gov/ACPI/Documents/ACPIfinal.html.

Pauly, D., and V. Christensen. "Primary production required to sustain global fisheries." Nature 374.6519 (1995): 255-257.

Pauly, D., et al. "The Peruvian upwelling ecosystem: Dynamics and interactions." The Peruvian upwelling ecosystem: dynamics and interactions. (1989): I-X, 1-438.

Pauly, D., and I. Tsukayama. "The Peruvian anchoveta and its upwelling ecosystem: Three decades of change." ICLARM (International Center for Living Aquatic Resources Management) Contribution (1987): I-XII, 1-351.

Philander, S. G. H. Our affair with El Niño: How we transformed an enchanting Peruvian current into a global climate hazard. 1st ed. Princeton, NJ, USA: Princeton University Press, 2006.

Philander, S. G. H., et al. "Why the ITCZ is mostly north of the equator." Journal of Climate 9.12 (1996): 2958-2972.

Philip, S., and G. J. Van Oldenborgh. "Shifts in ENSO coupling processes under global warming." Geophysical Research Letters 33.11 (2006): 5.

Picaut, J., et al. "Mechanism of the zonal displacements of the pacific warm pool: Implications for ENSO." Science 274.5292 (1996): 1486-1489.

Podesta, G. P., Browder, J. A., & Hoey, J. J. "Exploring the association between swordfish catch rates and thermal fronts on us longline grounds in the western north Atlantic." Continental Shelf Research 13.2-3 (1993): 253–277.

Quinn, W. H., V. T. Neal, and S. E. A. Demayolo. "El Niño occurrences over the past 4-1/2 centuries." Journal of Geophysical Research-Oceans 92.C13 (1987): 14449-14461.

Rayner, N. A., et al. "Global analyses of sea surface temperature, sea ice, and night marine air temperature since the late nineteenth century." Journal of Geophysical Research Atmospheres 108.D14 (2003).

Ryther, J. H. "Photosynthesis and fish production in sea." Science 166.3901 (1969): 72-76.

Santander, H. Distribution patterns and fluctuations in anchovy and sardine spawning., Callao, Peru.

Schneider, N., and B. D. Cornuelle. "The forcing of the Pacific Decadal Oscillation." Journal of Climate 18.21 (2005): 4355-4373.

Schwartzlose, R. A., et al. "Worldwide large-scale fluctuations of sardine and anchovy populations." South African Journal of Marine Science Suid Afrikaanse Tydskrif Vir Seewetenskap 21 (1999): 289-347.

Selten, F. M., et al. "Tropical origins for recent and future Northern Hemisphere climate change." Geophysical Research Letters 31.21 (2004): 4.

Shaffer, G., et al. "Circulation and variability in the Chile basin." Deep-Sea Research Part I - Oceanographic Research Papers 51.10 (2004): 1367-1386.

Shu, L. H., and A. J. Clarke. "Using an ocean model to examine ENSO dynamics." Journal of Physical Oceanography 32.3 (2002): 903-923.

Stenseth, N. C., et al. "Ecological effects of climate fluctuations." Science 297.5585 (2002): 1292-1296.

Sterl, A., et al. "On the robustness of ENSO teleconnections." Climate Dynamics 29.5 (2007): 469-485.

Strub, P. T., J. M. Mesias, V. Montecino, J. Rutllant, and S. Salinas. "Coastal ocean circulation off western South America." The Sea. Ed. A. R. Robinson and K. H. Brink. Vol. 11. Hoboken, N. J., USA: John Wiley, 1998. 273– 313.

Tarazona, J., and W. Arntz. "The Peruvian coastal upwelling system." Ecological Studies (2001): 229-244.

Timmermann, A. "Detecting the nonstationary response of ENSO to greenhouse warming." Journal of the Atmospheric Sciences 56.14 (1999): 2313-2325.

Timmermann, A. "Changes of ENSO stability due to greenhouse warming." Geophysical Research Letters 28.10 (2001): 2061-2064.

Tomczak, M., and J.S. Godfrey. Regional Oceanography, An Introduction. Oxford, G.B.: Pergamon, 1994.

Tsimplis, M. N., S. Bacon, and H. L. Bryden. "The circulation of the subtropical South Pacific derived from hydrographic data." Journal of Geophysical Research-Oceans 103.C10 (1998): 21443-21468.

Ulloa, O., et al. "Evolution and biological effects of the 1997-98 El Niño in the upwelling ecosystem off northern Chile." Geophysical Research Letters 28.8 (2001): 1591-1594.

Van der Lingen, C. D., Hutchings, L., Merkle, D., Van der Westhuizen, J. J., & Nelson, J. "Comparative spawning habitats of anchovy (Engraulis capensis) and sardine (Sardinops sagax) in the southern Benguela upwelling ecosystem." Spatial Processes and Management of Marine Populations. Ed. N. Bez G. H. Kruse, T. Booth, M. Dorn, S. Hills, R. N. Lipcius, D. Pelletier, C. Roy, S. J. Smith, & D. Witherell. Fairbanks: University of Alaska Sea Grant, AK-SG-01-02, 2001.

van Oldenborgh, G. J., S. Y. Philip, and M. Collins. "El Niño in a changing climate: A multi-model study." Ocean Science 1.2 (2005): 81-95.

Vargas, G., et al. "Enhancement of coastal upwelling and interdecadal ENSO-like variability in the Peru-Chile current since late 19th century." Geophysical Research Letters 34.13 (2007): 6.

Vecchi, G.A., A. Clement and B.J. Soden. "Examining the tropical pacific's response to global warming." EOS, Trans. Am. Geophys. Union 89.9 (2008): 81,83.

Vecchi, G. A., and B. J. Soden. "Global warming and the weakening of the tropical circulation." Journal of Climate 20.17 (2007): 4316-4340.

Vecchi, G. A., et al. "Weakening of tropical pacific atmospheric circulation due to anthropogenic forcing." Nature 441.7089 (2006): 73-76.

von Storch, H., and F.W. Zwiers. Statistical Analysis in Climate Research. 2nd. ed. Cambridge, UK: Cambridge University Press, 1999.

Wallace, J. M., T. P. Mitchell, and C. Deser. "The influence of sea-surface temperature on surface wind in the eastern equatorial pacific: Seasonal and interannual variability." Journal of Climate 2 (1989): 1500-1506.

Walsh, J. J., et al. "Spawning habitat of the Peruvian anchovy, Engraulis ringens." Deep Sea Research Part A - Oceanographic Research Papers 27.1 (1980): 1-27.

Wang, C., and J. Picaut. "Understanding ENSO physics - a review." Earth's climate: The ocean-atmosphere interaction. Ed. S.-P. Xie C. Wang, and J. A. Carton. Vol. 147. AGU Geophysical Monograph series: AGU Geophysical Monograph Series, 2004. 21-48.

Wang, C. Z., and P. C. Fiedler. "ENSO variability and the eastern tropical pacific: A review." Progress in Oceanography 69.2-4 (2006): 239-266.

Wang, W. M., and M. J. McPhaden. "The surface-layer heat balance in the Equatorial Pacific Ocean. Part II: Interannual variability." Journal of Physical Oceanography 30.11 (2000): 2989-3008.

Washington, W. M., et al. "Parallel climate model (PCM) control and transient simulations." Climate Dynamics 16.10-11 (2000): 755-774.

Wilks, D. S. Statistical Methods in the Atmospheric Sciences. 2nd ed: Academic Press, 2006.

Williams D., Collins Philip J., Rasch, Byron A., Boville, James J., Hack, James R., McCaa, David L., Williamson, Jeffrey T., Kiehl, Bruce Briegleb. Description of the NCAR Community Atmosphere Model (CAM 3.0). Ed. NCAR Technical notes. Vol. 1. Boulder, Colorado, USA: National Center for Atmospheric Research, 2004.

Williams, K. F. "Sea surface temperature maps to assist tuna fisheries off New South Wales, Australia." FAO fisheries technical paper 170. Ed. G. H. Tomczak. FAO, 1977. 38-55.

Wust, W.H. La pesca en el antiguo Perú. 1st ed. Lima, Peru: Wust Ediciones, 2006.

Wyrtki, K. "Teleconnections in equatorial pacific ocean." Science 180.4081 (1973): 66-68.

Wyrtki, K. "El Niño - Dynamic-response of equatorial pacific ocean to atmospheric forcing." Journal of Physical Oceanography 5.4 (1975): 572-584.

Xie, S. P. "On the genesis of the equatorial annual cycle." Journal of Climate 7.12 (1994): 2008-2013.

Xie, S. P. "Westward propagation of latitudinal asymmetry in a coupled ocean-atmosphere model." Journal of the Atmospheric Sciences 53.22 (1996): 3236-3250.

Xie, S. P., et al. "A regional ocean-atmosphere model for Eastern Pacific climate: Toward reducing tropical biases." Journal of Climate 20.8 (2007): 1504-1522.

Xie, S. P., and S. G. H. Philander. "A coupled ocean-atmosphere model of relevance to the ITCZ in the Eastern Pacific." Tellus Series A - Dynamic Meteorology and Oceanography 46.4 (1994): 340-350.

Yanez, E., et al. "Climate variability and pelagic fisheries in northern Chile." Progress in Oceanography 49.1-4 (2001): 581-596.

Yu, J. Y., and C. R. Mechoso. "Links between annual variations of Peruvian stratocumulus clouds and of SST in the Eastern Equatorial Pacific." Journal of Climate 12.11 (1999): 3305-3318.

Zhang, J. L., and W. D. Hibler. "On an efficient numerical method for modeling sea ice dynamics." Journal of Geophysical Research-Oceans 102.C4 (1997): 8691-8702.

Zhang, X. B., and M. J. McPhaden. "Wind stress variations and interannual sea surface temperature anomalies in the Eastern Equatorial Pacific." Journal of Climate 19.2 (2006): 226-241.